UC San Diego
UC San Diego Previously Published Works

Title

Targeting ROR2 homooligomerization disrupts ROR2-dependent signaling and suppresses stem-like cell properties of human breast adenocarcinoma.

Permalink

https://escholarship.org/uc/item/42416819

Journal

iScience, 28(1)

Authors

Leng, Feng
Huang, Jiajia
Wu, Liufeng
et al.

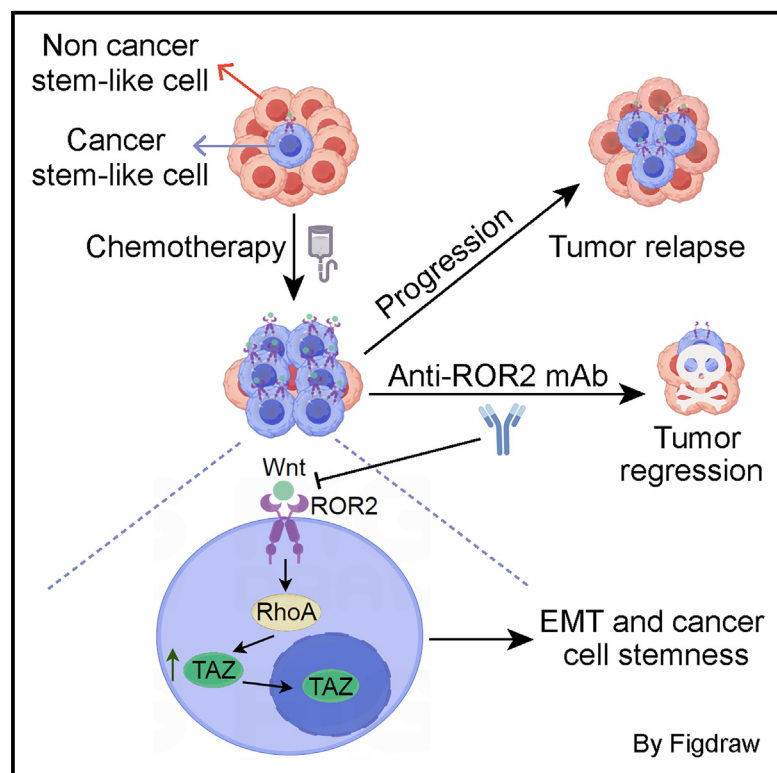**Publication Date**

2025-01-17

DOI

10.1016/j.isci.2024.111589

Peer reviewed

Article

Targeting ROR2 homooligomerization disrupts ROR2-dependent signaling and suppresses stem-like cell properties of human breast adenocarcinoma

Graphical abstract

Authors

Feng Leng, Jiajia Huang, Liufeng Wu, ..., Desheng Lu, Thomas J. Kipps, Suping Zhang

Correspondence

tkipps@health.ucsd.edu (T.J.K.), s9zhang@szu.edu.cn (S.Z.)

In brief

Stem cell plasticity; Molecular interaction; Cancer

Highlights

- Breast cancer cells with ROR2 expression have stem-like cell properties

- Expression of ROR2 promotes the acquisition of breast cancer stemness

- ROR2 homooligomerization is necessary for ROR2 activation in breast cancer

- An anti-ROR2 antibody inhibits ROR2 homooligomerization to suppress ROR2 signaling

CellPress

Article

Targeting ROR2 homooligomerization disrupts ROR2-dependent signaling and suppresses stem-like cell properties of human breast adenocarcinoma

Feng Leng,[1,5] Jiajia Huang,[2,5] Liufeng Wu,[1,5] Jianchao Zhang,[1] Xinxin Lin,[1] Ruhuan Deng,[1] Jinhang Zhu,[1] Zhen Li,[1] Zhenghao Li,[1] Yimeng Wang,[1] Han Zhang,[3] Desheng Lu,[1] Thomas J. Kipps,[4,*] and Suping Zhang[1,4,6,*]

[1]Shenzhen Key Laboratory of Precision Medicine for Hematological Malignancies, Guangdong Key Laboratory for Genome Stability and Human Disease Prevention, Department of Pharmacology, School of Basic Medical Sciences, Base for International Science and Technology Cooperation: Carson Cancer Stem Cell Vaccines R&D Center, International Cancer Center, Shenzhen University Medical School, Shenzhen University, Shenzhen 518055, China
[2]State Key Laboratory of Oncology in South China, Department of Medical Oncology, Collaborative Innovation Center for Cancer Medicine, Sun Yat-sen University Cancer Center, Guangzhou 510060, China
[3]Xenta Biomedical Science Co., Ltd, Guangzhou 510060, China
[4]Moores Cancer Center, University of California, San Diego, San Diego, CA 92037, USA
[5]These authors contributed equally
[6]Lead contact
*Correspondence: tkipps@health.ucsd.edu (T.J.K.), s9zhang@szu.edu.cn (S.Z.)
https://doi.org/10.1016/j.isci.2024.111589

SUMMARY

Breast cancer stem-like cells (CSCs) are enriched following treatment with chemotherapy, and posited as having a high level of plasticity and enhanced tumor-initiation capacity, which can enable cancer relapse. Here, we show that such features are shared by breast cancer (BCA) cells that express receptor tyrosine kinase-like orphan receptor (ROR2), which is expressed primarily during embryogenesis and by various cancers. We find that Wnt5a can induce ROR2 homooligomerization to activate noncanonical Wnt signaling and enhance tumor-initiation capacity of BCA cells. Molecular analysis reveals that the cysteine-rich domain and transmembrane domain are required for ROR2 homooligomerization to activate ROR2. Treatment with a newly generated monoclonal antibody (mAb) specific for ROR2 can block Wnt5a-induced ROR2 homooligomerization, ROR2-dependent noncanonical Wnt signaling, and impair the capacity of BCA patient-derived xenografts to initiate tumor in immune-deficient mice. Collectively, these results indicate that targeting ROR2 (e.g., using mAb) suppresses BCA stemness and, thereby, may prevent BCA relapse.

INTRODUCTION

Breast cancer (BCA) is among the most common cancers and the second leading cause of cancer-related deaths in women worldwide.[1] The disease has been classified by gene expression profiling into distinct subtypes: luminal A, luminal B, HER2-enriched (HER2+), and basal-like.[2] Despite initial response to treatment, many patients with BCA including luminal type BCA that have estrogen receptor (ER) expression can relapse and develop metastatic disease,[3] which is oftentimes intractable to therapy.[4] Accumulating evidence indicates that breast cancer stem-like cells (CSCs), also called tumor-initiating cells, are primarily responsible for development of therapy resistance ultimately resulting in cancer relapse and metastasis.[5–7] CSCs are able to survive antineoplastic therapy, have self-renewal and differentiation capacity and thus serve as clonogenic reserve for tumor regrowth.[8,9] Experimentally, BCA cells with such "stem-like" phenotype or stemness features generally have activated stem-like cell signaling (e.g., Hippo-YAP/TAZ),[10,11] expression of CD44 with low level CD24 (CD44+CD24Low), and the distinc-

tive capacity to form nonadherent cellular spheroids and engraft immune-deficient mice.[12–15] Moreover, such cells exhibit a high level of plasticity, a process by which cancer cells gain a "stem-like" cell phenotype in response to signaling from tumor microenvironment.[8,16,17] Hence, targeting signaling pathways that contribute to acquisition and/or maintenance of the "stem-like" cell properties may have attractive therapeutic potential.

Relevant in this regard is receptor tyrosine kinase-like orphan receptor 2 (ROR2), an evolutionarily conserved type I membrane protein that is expressed primarily during early development where it plays an important role in organogenesis.[18] The extracellular portion of ROR2 contains an extracellular immunoglobulin-like (Ig-like) domain, a kringle domain, and a cysteine-rich domain (CRD), which is common to frizzled proteins (FZDs), that can bind various wingless integrated (Wnt) factors, in particular Wnt5a.[19–21] The developmental significance of the binding of Wnt5a to ROR2 is underscored by studies on Wnt5a knockout mice, which exhibit developmental abnormalities similar to those of mice lacking ROR2, including dwarfish, facial deformities, shortened limbs and tails, dysplasia of lungs and genitals, and

ventricular septal defects.[18] Although important in early development, the expression of ROR2 attenuates postnatally and may remain at low level in some postpartum tissues (e.g., mammary tissues).[22–24] However, studies have shown that ROR2 expression is upregulated in various cancers, including BCA.[25–28] Expression of ROR2 in BCA may be associated with poor prognosis.[27,29,30] Moreover, ectopic expression of ROR2 on a BCA cell-line can induce the cells to undergo epithelial-to-mesenchymal transition (EMT),[29] a major contributing factor of CSCs plasticity,[31–33] suggesting that ROR2 expression might contribute to BCA stemness.

In this study, we evaluated the level of ROR2 expression in BCA of patients, and determined whether ROR2 expression can induce and/or maintain phenotypic and functional characteristics of breast CSCs. We also defined the mechanism underlying the activation of ROR2-dependent Wnt5a-induced signaling in BCA. Moreover, we generated a panel of monoclonal antibodies (mAbs) specific for ROR2, and identified one that could inhibit the activation of ROR2-dependent signaling, and the capacity of ROR2 to induce EMT or enhance engraftment of BCA patient-derived xenografts (PDXs).

RESULTS

Human BCA tumors with high *ROR2* express genes involved in CSCs

We interrogated the PubMed Gene Expression Omnibus (GEO) database (GSE87455) on breast tumor biopsies obtained from patients before and after neoadjuvant chemotherapy. We found that post-treatment biopsy specimens had significantly higher levels of *ROR2* than the matched pre-treatment tumor specimens ($n = 68$, $p < 0.001$) (Figure S1A). Interrogation of GSE21974 that also had breast tumor biopsies of patients ($n = 25$) before and after neoadjuvant chemotherapy yielded similar results (Figure S1A), confirming that the level of *ROR2* expression on post-treatment biopsies was significantly increased. Gene set enrichment (GSE) analysis revealed that comparing to pre-treatment BCA cells (GSE21974), post-treatment BCA cells had significantly higher level expression of genes associated with EMT activation ($p < 0.001$, FDR q value = 0.009; Figure S1B)[34] and genes that were distinctively over-expressed by CD44^{+}/CD24[Low] CSCs or mammosphere-(MS-) forming cells relative to CD44^{+}/CD24^{+} non-CSCs or all tumor cells ($p < 0.001$, FDR q value <0.001, Figure S1B),[12] which is consistent with prior analysis on GSE87455.[12,35] We further segregated the pretreatment specimens of GSE21974 into two subgroups based upon their relative expression of *ROR2*. Samples with *ROR2* levels greater than the median level expressed in all samples were designated as *ROR2*[Hi], whereas tumor samples with *ROR2* expression lower than the median level were designated as *ROR2*[Low]. The differences in gene expression between *ROR2*[Hi] versus *ROR2*[Low] breast tumors resembled those of matched post-versus pre-treatment specimens (Figure S1C). Moreover, segregation of gene expression data of invasive breast tumors, deposited in The Cancer Genome Atlas (TCGA) database, another large database ($n = 1097$), into two subgroups by virtue of their relative expression of *ROR2* yielded similar findings, identifying that *ROR2*[Hi] tumors expressed higher-level of genes

associated with EMT, CD44^{+}/CD24[Low] CSCs or MS-forming cells relative to *ROR2*[Low] tumors (Figure S1C).

### BCA PDX cells with ROR2 expression have stem-like cell features

To examine the relevance of ROR2 protein in BCA stemness, we collected fresh BCA clinical samples from treatment-naive patients and examined for ROR2 via immunoblot analysis using the H-1 anti-ROR2 antibody. The H-1 antibody that was raised against a synthetic peptide mapping at C-terminal-region (amino acids 868–943) of human ROR2,[36] specifically reacted with a protein of ≈ 120 kDa in lysates of HEK293T WT cells, but not ROR2-KO cells (Figure S2A). Moreover, 47 of 63 (75%) fresh-frozen tumor tissues including 25 of 31 (81%) luminal type BCA, 10 of 13 (77%) HER2^{+}, and 12 of 19 (63%) triple negative breast cancer (TNBC) also reacted with this antibody (Figure 1A). As receptor tyrosine-like orphan receptor 1 (ROR1) that can form heterooligomers with ROR2 is highly expresses by BCA stem-like cells.[35,37] We also examined these clinical specimens for ROR1 and noticed that more than half of ROR2-positive (ROR2^{+}) tumors lacked detetable ROR1 (Figure S2B).

We further made viable single-cell suspension from patients who had sufficient BCA biomaterials to engraft into NOD-*Prkdc*[em26Cd52]*IL2rg*[em26Cd22]/NjuCrl (NCG) immune-deficient mice. One of four established luminal type patient-derived xenografts (PDX IV) had tumor cells that expressed ROR1 and ROR2, whereas TNBC PDXIII had tumor cells that expressed ROR2 only (Figures 1B and S2C). Single cells isolated from PDXIII or PDXIV-that were treated with paclitaxel at 20nM for 48 h *in vitro*, or expressed CD44 and low-level CD24 had significantly enhanced ROR2 expression than did the same cells received control treatment or were CD44^{+}/CD24^{+}, respectively (Figures S2E and S2F), when assessed via flow cytometry using a commercially available anti-ROR2 mAb (clone # 231509) that can specifically react with HEK293T WT cells but not ROR2-KO cells (Figure S2D). On the other hand, ROR2^{+} cells isolated from PDXIII or PDXIV had higher proportions of CD44^{+}/CD24[Low] stem-like cells, enhanced mesenchymal marker expression (e.g., vimentin) than the same tumor cells that did not express ROR2 (Figures 1C–1E). Similarly, ROR2^{+} cells isolated from PDXIV had higher expression level of ROR1 than the same tumor cells that did not express ROR2 (Figure S2H).

Furthermore, ROR2^{+} tumor cells isolated from either PDXIII or PDXIV had an enhanced capacity to invade Matrigel, or form primary and secondary nonadherent cellular spheroids than did ROR2[Neg] tumor cells isolated from the same PDXs (Figures 1F and 1G). More importantly, extreme limiting dilution assay (ELDA) revealed that 100 ROR2^{+} cells from either PDXIII or PDXIVcould establish secondary PDXs in approximately half of the mice (Figure 1H). In contrast, the same numbers of ROR2[Neg] cells did not form tumors (Figure 1H). Collectively, these data indicate that ROR2 expression is associated with BCA stem-like cells, which may be independent of ROR1 expression.

ROR2 expression increases proportion of BCA stem-like cells and enhances engraftment of BCA cells

To evaluate ROR2 function in BCA stem-like cells, we transfected empty vector (EV) or vector encoding ROR2 into luminal
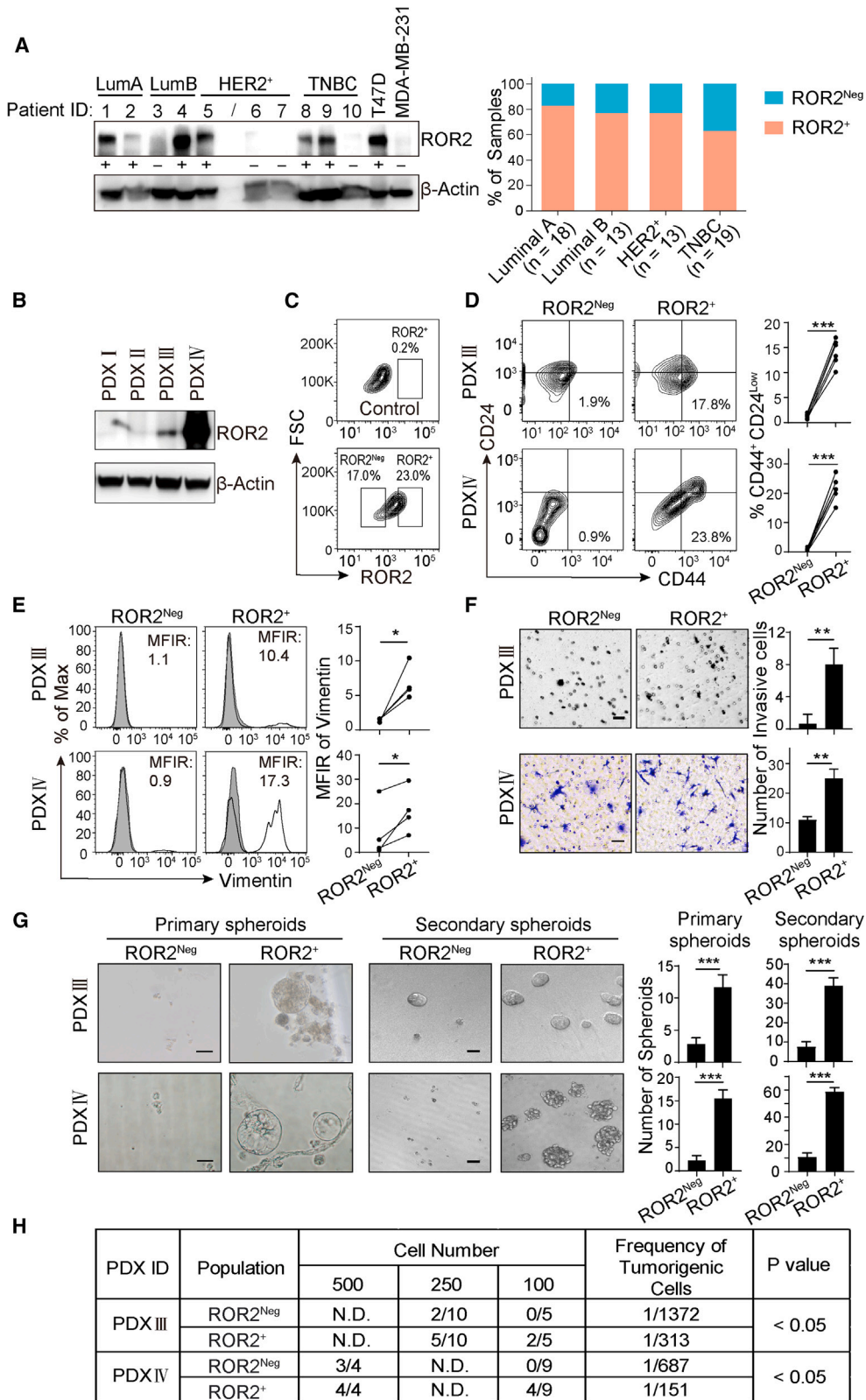
type BCA cell-line MCF7 that lacked both ROR1 and ROR2 expression or TNBC cell-line MDA-MB-231 that only lacked ROR2 expression (Figure S3A). Consistent with previous study,[29] ROR2-overexpressing MCF7 or MDA-MB-231 cells had reduced expression of an epithelial marker (E-cadherin), increased expression of mesenchymal markers (e.g., vimentin) and an enhanced capacity to invade Matrigel, and were more resistant to paclitaxel relative to EV-transfected MCF7, MDA-MB-231 cells or parental cells (Figures 2A, 2B, and S3B). Moreover, we found that ectopic expression of ROR2 in MCF7 cells could increase the proportion of CD44$^+$/CD24^{Low} stem-like cells and enhance the number of spheroids formed (Figures 2C and S3C). On the other hand, knocking out for ROR2 in luminal type T47D BCA cells that ordinarily have high-level expression of ROR2 but do not have ROR1 expression, increased expression of epithelial proteins (e.g., E-cadherin), decreased expression of mesenchymal markers (e.g., vimentin), reduced proportion of CD44$^+$/CD24^{Low} cells and reduced capacity to invade Matrigel or form spheroids, and made cells more sensitive to paclitaxel (Figures 2A–2C, S3B, and S3C).

To assess the tumor-initiation potential, we performed ELDA for T47D WT versus T47D ROR2-KO cells or MDA-MB-231 Vector versus ROR2-overexpressing cells. We found that injection of 1X10^6 ROR2$^+$ luminal type T47D WT cells into the mammary fat pads of NCG immune-deficient female mice was sufficient to generate mammary tumors in all mice. However, injection of this same number of T47D ROR2-KO cells generated mammary tumors in less than half of the injected mice (Figure 2D). Similarly, 500 ROR2^{neg} TNBC MDA-MB-231 cells could engraft in one of five NCG female mice while three of four mice formed tumors post-implantation of the same number of ROR2-overexpressing MDA-MB-231 cells (Figure 2D). Collectively, these data indicate that expression of ROR2 may induce and/or maintain stem-like features of BCA cells, in ROR1-independent manner.

ROR2 can form homooligomers to activate Rho-GTPase and Hippo-YAP/TAZ signaling in response to Wnt5a

To examine whether ROR2 can form homooligomers to activate noncanonical Wnt signaling to induce and/or maintain stem-like cells properties in BCA, we transfected vector encoding HA-tagged ROR2 or control protein toll-like receptor 5 (TLR5) alone, or together with vector encoding Flag-tagged ROR2 into HEK293T ROR2-KO cells, BCA cell-line MCF7 or MDA-MB-231 that lack ROR2 (Figures 3A, S3A, and S4A–S4C). Immunoprecipitation analysis using an anti-Flag antibody revealed that ectopically expressed ROR2 could oligomerize; this oligomerization of ROR2 could be enhanced by treatment with recombinant Wnt5a for 30 min in both HEK293T cells and MCF7 cells (Figures 3A and S4A). However, HA-tagged TLR5 could not pull-down Flag-tagged ROR2 (Figure S4B).

Consistent with previous studies in BCA,[35,38] treatment with exogenous Wnt5a could induce activation of RhoA and enhance expression of TAZ in ROR1-positive MDA-MB-231 cells (Figures 3B and 3C). Moreover, expression of ROR2 in MDA-MB-231 cells further enhanced RhoA activity and TAZ expression in response to Wnt5a stimulation (Figures 3B and 3C). Notably, exogenous Wnt5a also could induce activation of RhoA within 10 min in ROR1-negative MCF7 cells that over-expressed ROR2 but not in EV-transfected MCF-7 cells (Figure 3B). Treatment with Wnt5a for 4 h further enhanced expression and nuclear localization of TAZ in ROR2-overexpressing MCF7 cells but not in EV-transfected MCF7 cells (Figures 3C and 3D). Conversely, treatment of ROR2-positive T47D cells with Wnt5a induced activation of noncanonical Wnt signaling (e.g., RhoA) and increased expression and nuclear localization of TAZ (Figures 3B–3D). In contrast to its effect on T47D cells, Wnt5a no longer could induce activation of RhoA or increase expression and nuclear localization of TAZ in T47D ROR2-KO cells (Figures 3B–3D).

Figure 1. BCA PDX cells with ROR2 expression have stem-like cell features

(A) Lysates prepared from the fresh frozen breast tumor tissues of representative patients, T47D and MDA-MB-231 cells were evaluated for expression of ROR2 by immunoblot analysis. β-Actin serves as loading control. "+" or "-" below the first row indicates negative or positive for ROR2, respectively. The bar graph on the right provides the proportion of each BCA subtype found negative or positive for ROR2. The orange shading represents the proportion of cases that were ROR2-positive (ROR2$^+$) while the light blue shading indicates the proportion of cases that lack of ROR1 expression (ROR2^{Neg}). The number of different cases examined for each BCA subtype is indicated in the parentheses.

(B) Lysates from each of BCA PDXs were examined for ROR2 expression via immunoblot analysis. β-Actin serves as loading control.

(C–E) Cells from each PDX were stained with anti-ROR2, anti-CD44 and anti-CD24, anti-vimentin antibody, or an isotype-control mAb. (C) Strategy for gating ROR2$^+$ and ROR2^{Neg} cells. The open boxes indicate the gates used to select ROR2^{Neg} (left) or ROR2$^+$ (right) cells. (D) The contour plot in the left panel depict the fluorescence of anti-CD44 and anti-CD24 on gated ROR2$^+$ or ROR2^{Neg} PDX cells; The right panel provides the proportion of CD44-positive (CD44$^+$) CD24-low (CD24^{Low}) cells ($n = 6$ per PDX) in ROR2^{Neg} versus ROR2$^+$ BCA cells from each of different mice engrafted with PDXIII (upper) or PDXIV (lower). *** indicates $p < 0.001$, as determined by paired Student's t test. (E) The histograms depict the fluorescence of gated ROR2$^+$ or ROR2^{Neg} PDX cells when stained with anti-vimentin mAb (the open histograms) or an isotype-control mAb (the shaded histograms). The number in each histogram provides the mean fluorescence intensity ratio (MFIR) for vimentin, which is derived from the mean fluorescence intensity (MFI) of cells labeled with the anti-vimentin mAb divided by MFI of cells labeled with control mAb. The right panel provides the MFIR value of vimentin for ROR2$^+$ versus ROR2^{Neg} BCA cells from each of different mice ($n = 4$ per PDX) engrafted with PDXIII or PDXIV. * indicates $p < 0.05$, as determined by paired Student's t test.

(F) Photomicrographs of Matrigel-invading cells from ROR2$^+$ or ROR2^{Neg} cells isolated from PDXIII and PDXIV. Scale bar, 50 μm. The bar graph (right) depicts the means ± SD of the numbers of invasive cells in three independent experiments. ** indicates $p < 0.01$, as determined by Student's t test.

(G) Photomicrographs of primary and secondary spheroids formed from ROR2$^+$ or ROR2^{Neg} cells isolated from each of the PDX, as indicated on the left margin. Scale bar: 50 μm. The bar graph (right) depicts the average numbers of spheroids ±SD in three independent experiments. *** indicates $p < 0.001$, as determined by Student's t test.

(H) Tumor incidence in animals implanted with ROR2$^+$ or ROR2^{Neg} cells isolated from PDXIII and PDXIV. The numbers of injected tumor cells are indicated at the top of the columns, which provide the numbers of mice that developed tumor over the number of mice injected with indicated cell populations. Frequency of tumorigenic cells and probability estimates were computed using extreme limiting dilution assay (ELDA) software. N.D indicates not done. Also see Figure S2 and Tables S1 and S2.
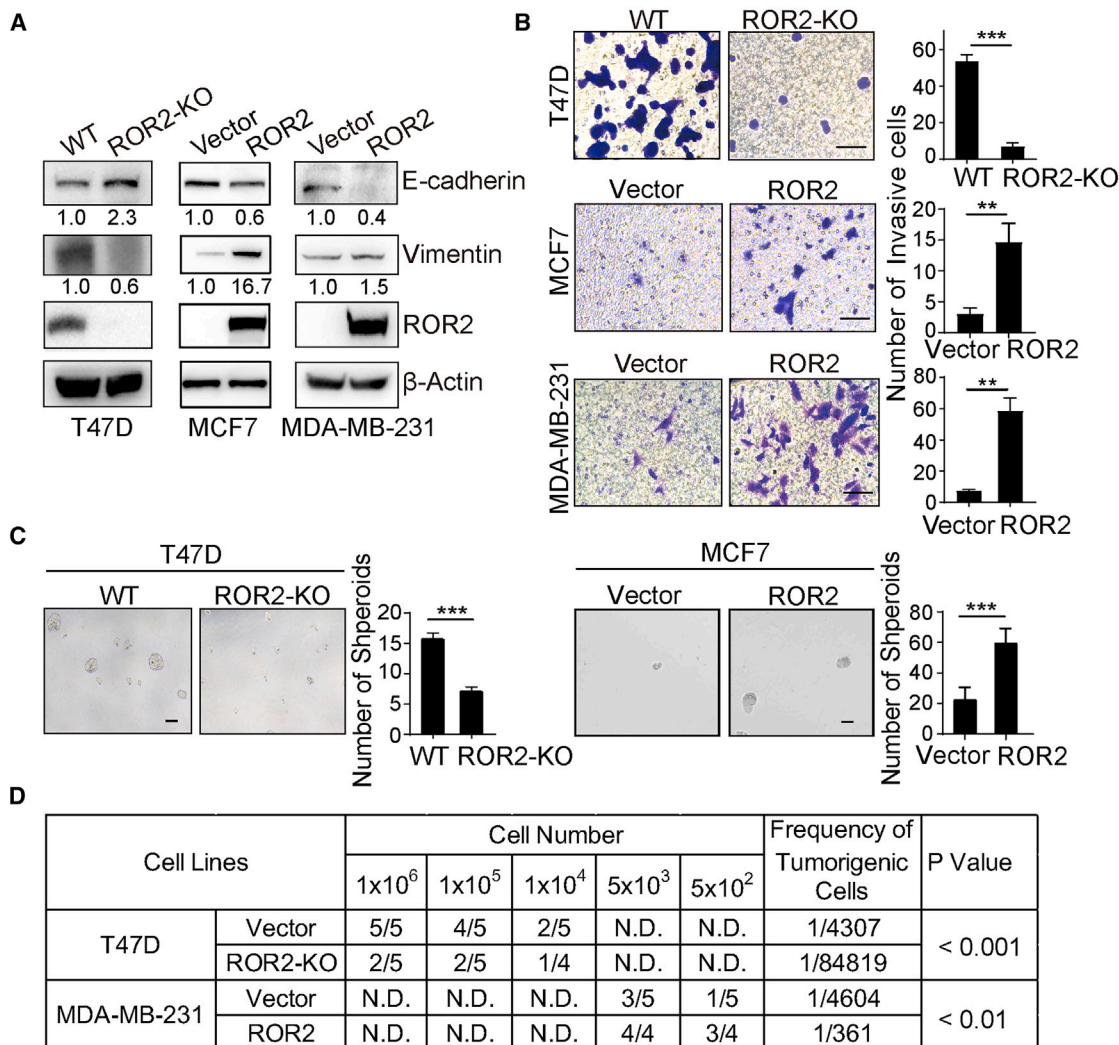
Figure 2. ROR2 expression increases proportion of BCA stem-like cells and enhances engraftment of BCA cells

(A) Immunoblot analysis for the indicated proteins using lysates prepared from T47D wild-type (WT) and ROR2 knockout (ROR2-KO) cells, or MCF7 and MDA-MB231 cells transduced with empty vector (Vector) or vector encoding ROR2 (ROR2). The numbers below each row are the ratios of the band densities of each protein relative to β-Actin, normalized with respect to that of the first control sample in each cell type.

(B) Representative photomicrographs depict the invasive cells from T47D WT versus ROR2-KO, and MCF7 vector versus ROR2 cells, and MDA-MB-231 vector versus ROR2 cells as indicated on the top. Scale bar: 50 μm. The histograms to the right of photomicrographs depict the average numbers of invading cells from T47D WT versus ROR2-KO, MCF7 vector versus ROR2 cells, and MDA-MB-231 vector versus ROR2 cells ±SD of one representative experiment of three independent experiments. ** indicates $p < 0.01$ and *** indicates $p < 0.001$, using Student's t test.

(C) Representative photomicrographs depict the spheroids from T47D WT versus ROR2-KO, and MCF7 vector versus ROR2 cells as indicated on the top. Scale bar: 50 μm. The histograms to the right of photomicrographs depict the average numbers of spheroids from T47D WT versus ROR2-KO, and MCF7 ector versus ROR2 cells ±SD of one representative experiment of three independent experiments. ** indicates $p < 0.01$ and *** indicates $p < 0.001$, using Student's t test.

(D) Table provides the numbers of mice that developed tumors (numerator) versus the numbers of mice (denominator) injected with varying numbers (as indicated in the row below "cell number") of T47D WT or ROR2-KO cells (as indicated in the left column). Frequency of tumorigenic cells and probability estimates were computed using ELDA software. Also see Figure S3.

Structural domains of ROR2 required for homooligomerization to activate ROR2

To map the domain which is required for ROR2 homooligomerization, we generated serial deletion mutants of ROR2 that each lacked one or more extracellular domains, or lacked the entire intracellular (ΔC) or extracellular (ΔN) domains (Figure 4A). We performed immunoprecipitation analysis in HEK293T ROR2-KO cells and found that all of these truncated forms of ROR2 including

ΔC and ΔN could still form homooligomers (Figure 4B), suggesting that the transmembrane domain (TMD) consisting of 21 amino acids (aa) common to all truncated mutant proteins may be sufficient to allow for ROR2 oligomerization. We replaced the TMD of each ROR2 truncation with the 19 aa TMD of human CD25 which was found expressing at the plasma membrane as a monomer[39] (Figures 4C and S4D). Confocal microscopy analysis confirmed that TMD-replaced Δ303 (Δ303-rTMD) ROR2 lacking both CRD
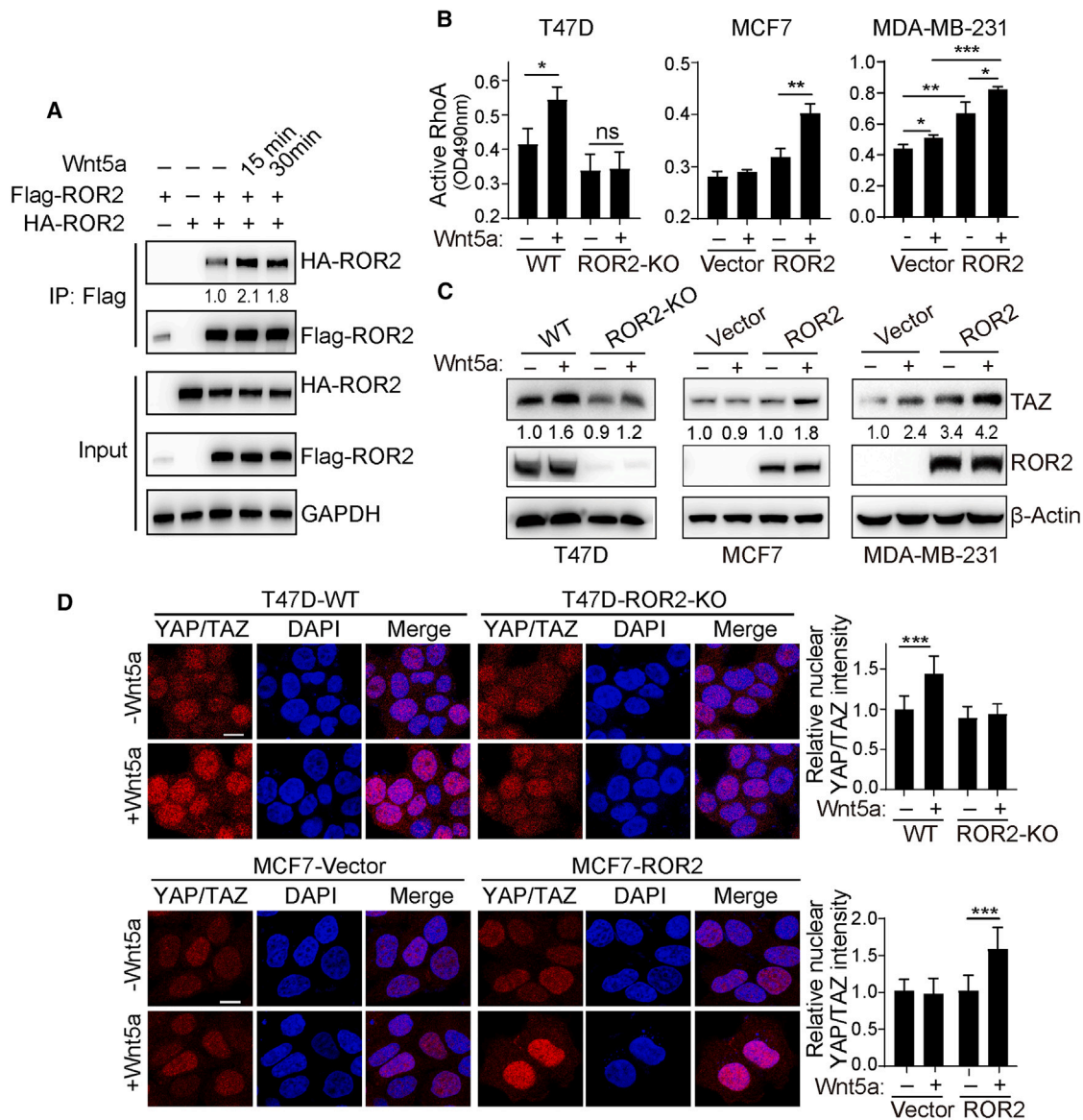
Figure 3. ROR2 can form homooligomers to activate Rho-GTPase and YAP/TAZ in response to Wnt5a

(A) MCF7 cells transfected with vector encoding Flag-tagged ROR2 (Flag-ROR2), and/or HA-tagged ROR2 (HA-ROR2) were cultured for 48 h and then were starved with serum-free medium for 6 h, following by addition with (+) or without (−) 150 ng/mL recombinant Wnt5a protein for the indicated time periods. Protein lysates prepared from each sample were immunoprecipitated (IP) with an anti-Flag antibody. The immune precipitates were evaluated by immunoblot analysis. The numbers below the first immunoblot represent the ratios of the band densities for indicated lane relative to cells cultured with serum-free medium lacking exogenous Wnt5a protein.

(B) The bar graphs depict RhoA activity in T47D WT and ROR2-KO cells, or MCF7 Vector and ROR2 cells, or MDA-MB-231 Vector or ROR2 cells that were stimulated with recombinant Wnt5a at 150 ng/mL for 10 min, as determined by enzyme-linked immunosorbent assay (ELISA). Data represent the mean values of triplicate wells ±SD of one representative experiment from three independent experiments. * indicates $p < 0.05$, ** indicates $p < 0.01$ and *** indicates $p < 0.001$, using Student's t test.

(C) Immunoblot analysis for TAZ and ROR2 proteins as indicated on the right using lysates prepared from T47D WT and ROR2-KO cells, MCF7 Vector and ROR2 cells, and MDA-MB-231 Vector and ROR2 cells which were treated with (+) or without (−) 150 ng/mL recombinant Wnt5a for 4 h. The numbers below each row represent the ratios of the band densities for each protein relative to that of β-Actin, normalized with respect to that of the first control sample in each cell type.

(D) Representative confocal images of T47D WT and ROR2-KO cells, or MCF7 Vector and ROR2 cells that were treated with or without 150 ng/mL Wnt5a for 6 h as indicated and then stained for YAP/TAZ and 4′,6-diamidino-2-phenylindole (DAPI) as indicated. Scale bar: 10 μm. The histogram to the Right of the photomicrographs provides the relative average intensity of YAP/TAZ located within the nuclei of the cells in each field ($n = 20$, ±SD). *** indicates $p < 0.001$, using Student's t test. Also see Figure S4.
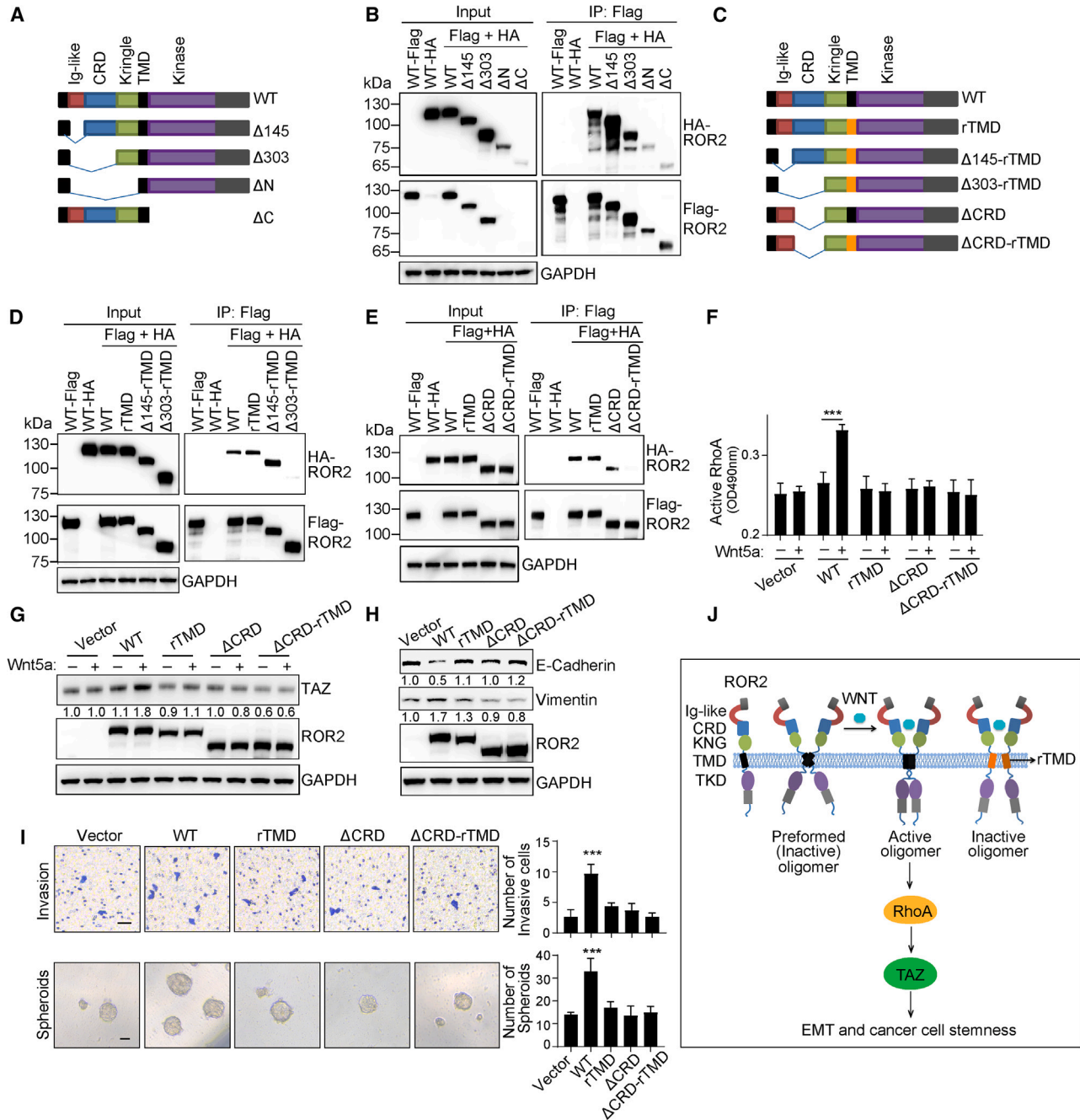
Figure 4. Structural domains of ROR2 required for homooligomerization to activate ROR2

(A) Schematic depicts the structure of wild-type (WT) or truncated forms of ROR2.

(B) Protein lysates of HEK293T cells transduced with vector encoding WT or each of truncated forms of Flag-ROR2 and/or HA-ROR2 were immunoprecipitated (IP) with anti-Flag antibody. The bound products or cell lysate input (input) was probed by immunoblot using either anti-Flag or anti-HA. GAPDH serves as loading control.

(C) Schematic depicts the structure of WT or mutated ROR2. rTMD represents that transmembrane domain (TMD) of ROR2 is replaced with TMD of CD25.

(D-E) HEK293T cells transduced with vector encoding WT or each of mutants of Flag-ROR2 and/or HA-ROR2 were lysed for immunoprecipitation (IP) with anti-Flag antibody, followed by immunoblot analyses with anti-Flag or anti-HA antibody. GAPDH serves as loading control.

(F) T47D ROR2-KO transduced with empty vector (Vector) or vector encoding WT or each of ROR2 mutants were stimulated with recombinant Wnt5a at 150 ng/mL for 10 min. RhoA activation was measured by ELISA and data show the mean values of triplicate wells ±SD of one representative experiment from three independent experiments. *** indicates $p < 0.001$, as assessed by Student's t test.

(legend continued on next page)

and Ig-like domain still retained on the cytoplama membrane (Figure S4E). However, Immunoprecipitation analysis revealed that this mutant failed to form homooligomers, while TMD-replaced Δ145 (Δ145-rTMD) ROR2 lacking only the Ig-like domain still could form homooligomers (Figure 4D), suggesting that CRD might also contribute to ROR2 oligomerization. Therefore, we generated truncated forms of ROR2 lacking the CRD domain with (ΔCRD-rTMD) or without replacement of CD25 TMD (ΔCRD) (Figure 4C). Indeed, ΔCRD-rTMD ROR2 that located on the cytoplasma membrane failed to oligomerize while ΔCRD ROR2 truncation form or mutant that had TMD replaced with CD25 TMD (rTMD) on the cytoplama membrane still could oligomerize (Figures 4E and S4E). However, the rTMD mutant did not display enhanced homooligomerization in response to Wnt5a stimulation, although the rTMD but not ΔCRD ROR2 mutant had the capacity to bind to Wnt5a (Figures S4F and S4G). Taken together, these findings suggest that both CRD and TMD contribute to ROR2 oligomerization and activation.

We also transduced T47D ROR2-KO BCA cells with vector encoding WT, ΔCRD, rTMD or ΔCRD-rTMD ROR2, respectively. We noted that WT ROR2 expression could re-activate RhoA and enhance TAZ expression in response to Wnt5a in T47D ROR2-KO cells whereas ΔCRD-rTMD ROR2 mutant expression failed to do so (Figures 4F and 4G). Interestingly, neither ΔCRD nor rTMD ROR2 mutant expression was able to re-activate RhoA or enhance TAZ expression in T47D ROR2-KO cells upon treatment of exogenous Wnt5a (Figures 5F and 5G), although these two mutants could form homooligomers. These data imply that homooligomers formed by ΔCRD or rTMD ROR2 might be functionally inactive.

Indeed, T47D ROR2-KO cells expressing WT ROR2 had decreased expression of epithelial proteins (e.g., E-cadherin), increased mesenchymal markers (e.g., vimentin) expression, and an enhanced capacity to invade Matrigel and form spheroid relative to the same cells transduced with EV (Figures 4H and 4I). However, expression of ΔCRD, rTMD or ΔCRD-rTMD ROR2 mutant could not interfere with expression of EMT markers, invasive or spheroid formation capacity in BCA cells (Figures 4H and 4I). Collectively, these data support a model that the ligands (e.g., Wnt5a) of ROR2 may induce ROR2 to form activated homooligomers that activate noncanonical Wnt signaling (e.g., RhoA), leading to up-regulation of TAZ expression, induction of EMT and BCA cell stemness; this process requires both CRD and TMD of ROR2 (Figure 4J).

An anti-ROR2 mAb can block Wnt5a-induced ROR2 homooligomerization, activation of Rho-GTPase and YAP/TAZ, and reduce the capacity of BCA cells to invade Matrigel or form spheroids

We generated 20 chimeric anti-ROR2 mAbs specific for the extracellular portion of ROR2 as assessed via enzyme-linked immunosorbent assay (ELISA) (Figure S5A). Four mAbs, designated as A12, B22, B30 and B16, that had high binding affinity to ROR2 extracellular portion also could specifically react to surface ROR2 on T47D WT cells but not T47D ROR2-KO cells (Figures 5A and S5A). Treatment with B22, B30 or B16 at 50 μg/mL, respectively, significantly reduced the invasion capacity of T47D cells in vitro. However, A12 mAb that had a less binding affinity to the ROR2-ECD than did B16 had no effect on cell invasion (Figures 5B and S5A). As it appears that B16 inhibited invasion capacity of T47D the most among these mAbs (Figure 5B), we selected it for further analyses.

Similarly, B16 also inhibited the invasion capacity of ROR2-overexpressing MDA-MB-231 (Figure 5C). More interestingly, we found that that B16 could block the interaction of ROR2 and Wnt5a in HEK293T ROR2-KO cells that co-transfected with Flag-tagged ROR2 and HA-tagged Wnt5a, as assessed via immunoprecipitation analysis (Figure 5D). To examine the effect of B16 on ROR2 homooligomerization and avoid the cross-linking of Flag-tagged ROR2 with HA-tagged ROR2 by B16 whole antibody in immunoprecipitation assay, we generated B16 single-chain variable fragment (scFv). Similar to the whole antibody, B16 scFv reacted with T47D WT cells but not with ROR2-KO cells (Figure S5B). B16 scFv was also able to inhibit the capacity of T47D cells to invade Matrigel (Figure S5C). B16 scFv could inhibit exogenous Wnt5a-induced homooligomerization of ROR2, as assessed via immunoprecipitation analysis (Figure 5E). As such, we observed that treatment with B16 inhibited Wnt5a-induced activation of RhoA and up-regulation of TAZ, up-regulated expression of epithelial cell markers (e.g., E-cadherin) and downregulated expression of mesenchymal cell markers (e.g., vimentin) (Figures 5F–5H), and the capacity of ROR2+ BCA cells to form primary and secondary spheroids (Figure 5I).

The anti-ROR2 mAb inhibits re-engraftment of BCA PDXs

To examine the activity of the anti-ROR2 mAb B16 in vivo, we treated mice engrafted with either PDXIII or PDXIV with intravenous infusions of B16 or control antibody at 10 mg/kg twice a

(G) T47D ROR2-KO cells expressing WT or mutated ROR2 (right) were stimulated with 150 ng/mL recombinant Wnt5a for 4 h. TAZ expression was evaluated via immunoblot analysis. GAPDH serves as loading control. The numbers below each lane represent the ratio of the band density for each protein relative to that of GAPDH, normalized with respect to that of the first control sample.

(H) Immunoblot analysis for the indicated proteins using lysates prepared from T47D ROR2-KO cells transduced with empty vector (Vector) or vector encoding WT or each mutant of ROR2 as indicated on the top. The number below each lane represent the ratio of the band density for each protein relative to that of GAPDH, normalized with respect to that of the first control sample.

(I) Representative photomicrographs of the invasive cells (top) or the spheroids (bottom) from T47D ROR2-KO cells transduced with empty vector (Vector) or vectors encoding WT or mutants of ROR2 as indicated on the top. Scale bar: 50 μm. The histograms to the right of photomicrographs depict the average numbers of invading cells or spheroids from each of samples ±SD of one representative experiment of three independent experiments. *** indicates p < 0.001, using Dunnett's multiple comparison test.

(J) A schematic model for ROR2 promoting EMT and cancer cell stemness. In the absence of ROR2 ligand (e.g., Wnt5a), ROR2 is present as monomer or forming inactive homooligomer via the TMD domain. In the presence of its ligand that is expressed by tumor cells or tumor microenvironment (e.g., stromal cells), ROR2 forms active homooligomer to activate noncanonical Wnt signaling (e.g., RhoA) to up-regulate TAZ expression, resulting in induction of EMT and cancer cell stemness. Of note, if TMD of ROR2 is replaced with TMD of CD25 (rTMD), ROR2 may form inactive homooligomers. Also see Figure S4.
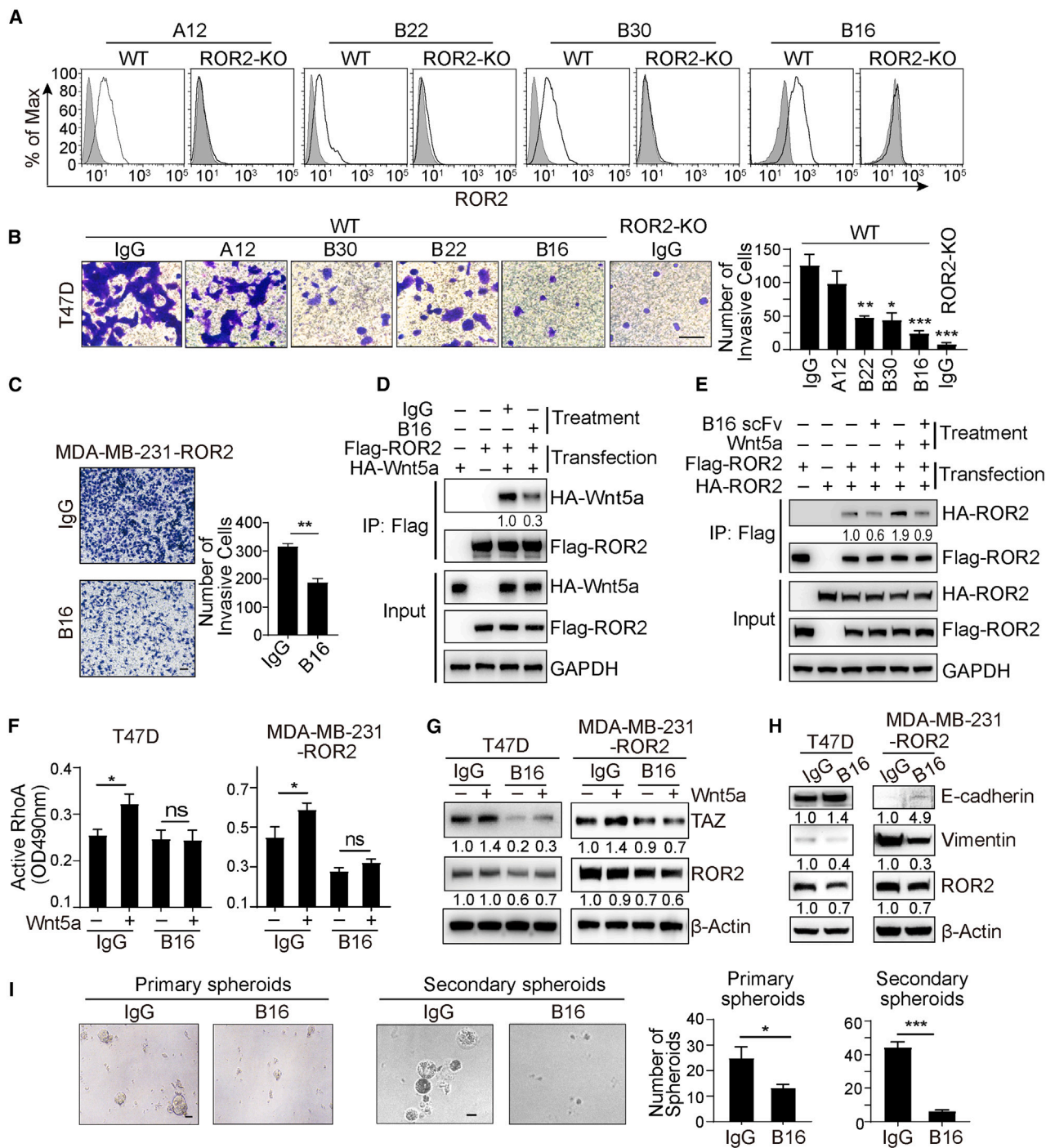
Figure 5. An anti-ROR2 mAb can block Wnt5a-induced ROR2 homooligomerization, activation of Rho-GTPase, reverse EMT, and reduce the capacity of BCA cells to invade Matrigel or form spheroids

(A) Histograms depict the fluorescence of T47D WT or ROR2-KO cells stained with A12, B22, B30 or B16 (open histograms), or isotype-control mAb of irrelevant specificity (shaded histograms), respectively.

(B) Representative photomicrographs of invading T47D ROR2-KO or WT cells that were treated with control IgG or indicated anti-ROR2 mAbs at 50 μg/mL. Scale bar: 50 μm. The bar graph to the right indicates the average numbers of invading cells from each of samples ±SD of one representative experiment of three independent experiments. * indicates $p < 0.05$, ** indicates $p < 0.01$ and *** indicates $p < 0.001$, using Dunnett's multiple comparison test.

(legend continued on next page)

week and found that B16 significantly suppressed the development and growth of both PDXIII or PDXIV tumors (Figures 6A and S6A). We further examined the transcriptomes of BCA PDXIII and PDXIV excised from control-IgG-treated mice ($n = 4$) and B16-treated mice ($n = 4$), respectively, and performed GSE analysis on the RNA-seq data (GEO: GSE191159). We found that tumor cells isolated from BCA PDXs of B16-treated mice expressed significantly lower levels of genes associated with β-catenin dependent canonical Wnt (Wnt/β-catenin) signaling, non-canonical Wnt signaling, AVB3 integrin, focal adhesion, TGF-β, Hedgehog, AP-1, Rho-GTPase, Notch, JNK MAPK pathways compared with the PDX cells from control-IgG-treated mice (Figure 6B). Notably, expression level of genes associated with the activation of Rho-GTPase or EMT and genes over-expressed by CD44$^+$/CD24^{Low} CSC or MS-forming cells were also significantly lower on PDX cells isolated from B16-treated mice than that on the PDX cells from control mice. Consistently, the PDXs of B16-treated mice had reduced RhoA activity and TAZ expression, decreased mesenchymal (e.g., vimentin), and increased epithelial (e.g., E-cadherin) expression by immunoblot analyses, together with reduced proportions of ROR2$^+$ and CD44$^+$/CD24^{Low} cells by flow cytometry analysis when compared with matched PDXs excised from control-treated mice (Figures 6C–6F). Given the substantial reduction in tumor volume following B16 treatment, we assessed tumor cell proliferation and apoptosis in PDXs tissues using Ki67 staining and caspase 3 cleavage assay, respectively. We found that B16 treatment did not significantly alter tumor cells proliferation whereas it did induce caspase 3 cleavage (Figures S6B and S6C), indicating that B16 may impair tumor cell survival.

Finally, we examined PDX cells from control-treated and B16-treated mice for their capacity to form secondary PDXs in immune-deficient mice. PDX cells isolated from B16-treated mice were significantly less effective in forming secondary PDXs than tumor cells of the same PDXs isolated from mice treated with IgG (Figure 6G). The frequency of tumorigenic cells in the PDXs from B16-treated mice was less than one-tenth that of control-treated mice (Figure 6G). Collectively, these data indicate that treatment with B16 can inhibit the capacity of ROR2$^+$ BCA to generate secondary tumors, an important facet of CSCs.

DISCUSSION

The central properties of CSCs with respect to their capacity of tumor initiation and plasticity clearly place them at the center for developing resistance to conventional anti-cancer therapy.[7,40] Thus, targeting CSCs should consider the mechanisms and factors leading to CSC conversion and/or maintanance. Here, we demonstrate that ectopic expression of ROR2 can generate CD44$^+$CD24^{Low} BCA stem-like cells, increase the capacity of BCA cells to form spheroids and engraft immune-deficient mice. Conversely, knocking out for ROR2 in ROR2$^+$ BCA cells induces the loss of BCA stem-like cell properties, as evidenced by reduction of number of CD44$^+$CD24^{Low} stem-like cells, reduced capacity of BCA cells to form spheroids and engraft immune-deficient mice, suggesting that ROR2 expression may activate stem-like cell signaling to convert non-CSCs to CSCs and/or maintain BCA stem-like cell properties. As such, we observed that enhanced expression of ROR2 in residual tumor cells surviving chemotherapy activates CSCs signaling, making BCA cells more resistant to chemotherapy relative to BCA cells lacking of ROR2 expression, which is consistent with a prior study showing an elevated Wnt5a expression and its activated signaling post-chemotherapeutic treatment for BCA.[41]

Prior studies found that ROR2 can form heterooligomers with its homologous ROR1 to modulate synapse formation in hippocampal neurons.[42] Here, we find that high ROR2 is expressed in high proportion of each BCA subtype, which is distinctive from ROR1 that is more prevalent in TNBC (57%) relative to luminal subtype (12%) or HER2$^+$ tumors (0%), as reported previously.[43] Moreover, expression of ROR2 can enhance the capacity of ROR1-negative BCA cells[44] to form spheroids and engraft immune-deficient mice. These data are consistent with our recent

(C) Representative photomicrographs of invading MDA-MB-231-ROR2 cells that were treated with control IgG or B16 antibody at 50 μg/mL. Scale bar: 50 μm. The bar graph to the right indicates the average numbers of invading cells from each of samples ±SD of one representative experiment of three independent experiments. ** indicates $p < 0.01$ using Student's t test.

(D) HEK293T ROR2-KO cells transfected with vector encoding Flag-ROR2, and/or HA-Wnt5a were cultured for 42 h and then were treated with or without B16 at 40 μg/mL for 6 h. Protein lysates prepared from each sample were immunoprecipitated (IP) with anti-Flag beads. The immune precipitates were evaluated by immunoblot analysis. The numbers below the first immunoblot represent the ratios of the band densities for indicated lane relative to third lane.

(E) HEK293T ROR2-KO cells transfected with vector encoding Flag-ROR2, and/or HA-ROR2 were cultured in medium with serum for 48 h and then were starved with serum-free medium supplemented with or without B16 single-chain variable fragment (scFv) at 40 μg/mL for 6 h, followed by addition with (+) or without (−) 150 ng/mL recombinant Wnt5a protein for 30 min. Protein lysates prepared from each sample were immunoprecipitated (IP) with anti-Flag beads. The immune precipitates were evaluated by immunoblot analysis. The numbers below the first immunoblot represent the ratios of the band densities for indicated lane relative to third lane.

(F–G) T47D or MDA-MB-231 ROR2 cells were treated with B16 or control IgG at 50 μg/mL for 24 h and were stimulated with recombinant Wnt5a at 150 ng/mL for 10 min (F) or 4 h (G). RhoA activation (F) or TAZ expression (G) from each of samples was evaluated by ELISA or immunoblot analysis. The bar graphs in (F) show the mean values of triplicate wells ±SD of one representative experiment from three independent experiments. * indicates $p < 0.05$, as assessed via Student's t test. The number below each lane in (G) represents the ratio of the band densities for each protein relative to that of GAPDH, normalized with respect to that of the first control sample.

(H) Lysates prepared from T47D or MDA-MB-231 ROR2 cells that were treated with 50 μg/mL IgG or B16 for 24 h, respectively, were examined for indicated protein expression via immunoblot analysis. The number below each lane represents the ratio of the band densities for each protein relative to that of GAPDH, normalized with respect to that of control IgG-treated sample.

(I) Representative photomicrographs depict the primary and secondary spheroid from T47D cells treated with B16 or control IgG at 50 μg/mL for 10 days. Scale bar: 50 μm. The histograms to the right of photomicrographs depict the average numbers of spheroids from T47D cells ±SD of one representative experiment of three independent experiments. * indicates $p < 0.05$ and *** indicates $p < 0.001$ using Student's t test. Also see Figure S5.
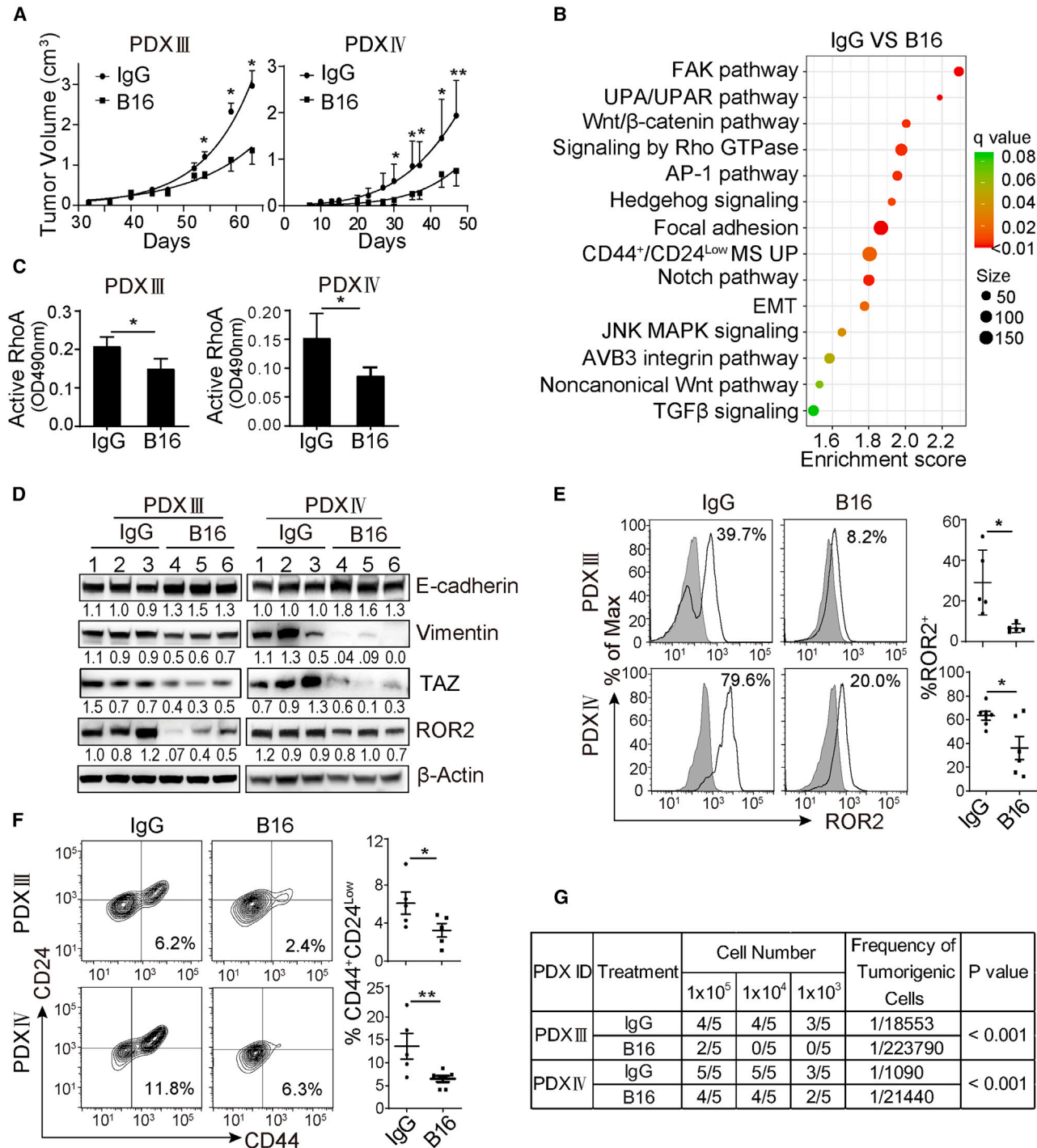
Figure 6. The anti-ROR2 mAb inhibits re-engraftment of BCA PDXs

(A–F) 1×10^6 single cell suspension of PDXIII and PDXIV were injected into the second mammary fat pads of female NCG mice. 10 mg/kg control IgG or anti-ROR2 mAb B16 were administered via intravenous injection twice a week and tumor growth was monitored. (A) The line graph depicts the mean tumor volume of BCA PDXIII and PDXIV over time from B16-treated animals or control-treated animals $\pm$SD ($n = 6$). * indicates $p < 0.05$ and ** indicates $p < 0.01$, using Student's t test. (B) Bubble plot of each of significantly activated signaling pathways or gene signatures in PDXIII and PDXIV tumor cells from control-treated mice versus B16-treated mice as assessed via RNA sequencing (RNA-seq) (GSE191159). Numbers on the right of color bar denote the false discovery rate (FDR) q value of an enriched gene set in control samples relative to B16-treated samples and numbers on the right of black bubbles indicates the number of genes in each gene set. (C) The bar graphs depict the mean RhoA activity $\pm$SD in PDXIII and PDXIV isolated from control-treated mice versus B16-treated mice, as determined by ELISA. * indicates $p < 0.05$, using Student's t test.

analysis at RNA level in I-SPY 2 BCA study showing that high *ROR2* or high *ROR1* distinctly identify subsets of BCA patients with adverse outcome,[45] implying ROR2 might activate downstream signaling in ROR1 independent manner in BCA.

Indeed, we find that Wnt5a can induce ROR2 homooligomerization to activate Rho-GTPase and Hippo-YAP/TAZ, independent of ROR1. Two models have been proposed for ligand-induced receptor triggering the induction of downstream signaling from monovalent ligand-binding receptors. In some cases, ligand binding can induce the formation of homotypic or heterotypic dimers or multimeric complexes, either directly, because the ligand itself is multimeric, or indirectly by inducing a conformational change in the receptor that reveals an intrinsic interaction motif.[46–48] Alternatively, monovalent receptors may exist in a preformed oligomer form and ligand binding induces a conformational change that is transduced through the TMD.[49,50] It appears that ROR2 pre-assembles into homotypic oligomers in the absence of its ligands, given that ΔCRD ROR2 mutant that lacks the ligand-binding domain remained as homooligomers. Moreover, despite having the capacity of binding to Wnt5a, expression of rTMD ROR2 that retained in homooligomer form also failed to activate ROR2-dependent signaling. These observations argue that oligomer conformation change might be necessary for ROR2 signaling in BCA, which could be supported by recent crystal structure analysis showing the presence of the inactive conformation for pseudokinase domain of ROR2.[51] Nevertheless, we could not exclude the possibility that replacing the ROR2 TMD with monomeric CD25 TMD might disrupt interaction of ROR2 with other proteins, potentially interfering with ROR2 activation.

Wnt factors (e.g., Wnt5a) might be able to induce conformation changes of ROR2 homooligomers to activate ROR2-dependent signaling. Consequently, BCA cells expressing Wnt5a[52,53] or treated with exogenous Wnt5a, in presence of WT ROR2 can activate Rho-GTPase, Hippo-YAP/TAZ, increase proportion of CD44$^+$CD24^{Low} breast CSCs and enhance the capacity of BCA cells for tumor initiation. However, despite retaining in homoligomer form, expression of ΔCRD ROR2 mutant that is unable to response to Wnt factors failed to do so. These data indicate that activated ROR2 homooligomers are required to activate ROR2-dependent signaling, maintain or induce BCA stem-like and/or mesenchymal phenotype. Consistent with this notion, a previous study found that ROR2 homooligomers in response to Wnt5a causes receptor autophosphorylation and induces functional consequences during osteogenesis.[20]

In any case, ROR2 expression in BCA cells can form activated homooligomers to activate Rho-GTPase in response to Wnt5a, leading to activation of Hippo-YAP/TAZ, which is consistent with previous report.[54] YAP, in turn, may upregulate Wnt5a and integrin alpha v which can induce TGF-β signaling.[55] Thus the noncanonical Wnt, TGF-β and Hippo-YAP/TAZ signaling cascades interact with each other to promote EMT to drive the mesenchymal CSCs signaling network. Consistent with this notion, we find that the anti-ROR2 mAb B16 may block the binding of ROR2 to Wnt5a, resulting in inhibition of Wnt5a-induced ROR2 homooligomerization, suppression of RhoA and TAZ activity in ROR2$^+$ BCA. Moreover, BCA PDX tumors isolated from mice treated with this mAb have reduced level of expression of genes associated with Wnt/β-catenin signaling, noncanonical Wnt, TGF-β signaling, EMT, CD44$^+$CD24^{Low} CSCs or MS-forming cells relative to the same tumors isolated from control-treated mice. Therefore, such mAb is able to reverse EMT, and inhibit the capacity of BCA cells to form spheroids, invade Matrigel, or engraft immune-deficient mice. Furthermore, treatment of primary breast PDX tumor cells with B16 impaired the capacity of tumor xenografts to re-engraft a virgin mouse. These studies demonstrate that the treatment with this anti-ROR2 mAb could inhibit CSCs signaling, impair EMT, the maintenance and/or the self-renewal capacity of CSCs, which otherwise may be resistant to conventional anti-cancer therapy and responsible for relapse after conventional anti-cancer treatment.[5,31,32]

Overall, our findings provide a rationale for the clinical evaluation of anti-ROR2 relevant treatment for patients with ROR2$^+$ BCA or other ROR2-expressing cancers. We speculate that B16 or other agents that can inhibit ROR2 signaling may enhance the survival of patients with ROR2-expressing BCA.

Limitations of the study

In response to ligand stimulation, ROR2 may undergo a conformational change to activate downstream signaling, which needs to be further demonstrated by protein structure analysis. Moreover, aside from preventing the receptor binding to the ligand, the anti-ROR2 antibody B16 may reduce the expression of ROR2 in BCA cells. The mechanism underlying this effect has not been investigated in this study.

RESOURCE AVAILABILITY

Lead contact

(D) Immunoblot analysis for proteins as indicated on the right using lysates from PDXIII and PDXIV that were excised from mice received control IgG or B16 treatment. The numbers below each row represent the ratios of the band densities for each protein relative to that of β-Actin, normalized to the average of IgG-treated each PDX.

(E) The histograms on the left depict the fluorescence of PDX tumor cells stained with anti-ROR2 mAb (open histograms), or control mAb of irrelevant specificity (shaded histograms), respectively.

(F) The contour plots depict the fluorescence of PDX tumor cells stained with anit-CD44 and anit-CD24 antibody. The scatterplot on the right shows the average proportion of ROR2$^+$ (E) or CD44$^+$/CD24^{Low} cells (F) in each tumor population ±SD ($n = 5$). * indicates $p < 0.05$ and ** denotes $p < 0.01$, using Student's t test.

(G) Tumor incidence in animals implanted with cells from PDXIII or PDXIV (as indicated in the left column), which were removed from mice treated with either IgG or B16 (as indicated in the second column). The numbers of injected tumor cells are indicated at the top of the columns, which provide the numbers of mice that developed tumor over the number of mice injected with indicated cell populations. The frequency of tumorigenic cells and the probability estimates were computed using ELDA software. Also see Figure S6.

CellPress
OPEN ACCESS

Materials availability

All biological materials used in this study are available from the lead contact upon request or from commercial sources.

Data and code availability

- RNA-seq data have been deposited at NCBI GEO and are publicly available as of the date of publication. Accession number is listed in the key resources table. This paper analyzes existing, publicly available data. These accession website for the datasets are listed in the key resources table. Original western blot images and microscopy data reported in this paper will be shared by the lead contact upon request.
- The paper does not involve the development of custom computer code and therefore does not report any original code. All softwares used in this study are listed in the key resources table.
- Any additional information required to reanalyze the data reported in this paper is available from the lead contact upon request.

AUTHOR CONTRIBUTIONS

Conceptualization: S.Z. and F.L., Methodology: J.H., L.W., and H.Z. Investigation: F.L., J.H., L.W., X.L., R.D., J.Zhang, J.Zhu, Z.L., and Y.W. Visualization: F.L., J.H., and Z.L. Supervision: T.J.K. and S.Z. Writing—original draft: F.L., S.Z., and J.Zhang. Writing—review and editing: D.L., S.Z., and T.J.K.

DECLARATION OF INTERESTS

The authors declare no competing interests. L.W. and J.Zhang are currently working at School of Medicine, Southern University of Science and Technology, Shenzhen 518055, P.R. China.

STAR★METHODS

Detailed methods are provided in the online version of this paper and include the following:

- KEY RESOURCES TABLE
- EXPERIMENTAL MODEL AND STUDY PARTICIPANT DETAILS
  - Human samples
  - Animals
  - Cell culture
- METHOD DETAILS
  - Animal study
  - RNA-sequencing and data analysis
  - Gene set enrichment analyses
  - Plasmids
  - CRISPR/Cas9 genome editing
  - Immunoblot analysis
  - Immunohistochemical staining
  - Confocal immunofluoresence analysis
  - Flow cytometry analysis
  - RhoA activation assay
  - Cell invasion assay
  - Cell viability assay
  - Spheroid formation assay
  - Generation of chimeric mouse/human mAbs
- QUANTIFICATION AND STATISTICAL ANALYSIS

SUPPLEMENTAL INFORMATION

Supplemental information can be found online at https://doi.org/10.1016/j.isci.2024.111589.

REFERENCES

1. Bray, F., Ferlay, J., Soerjomataram, I., Siegel, R.L., Torre, L.A., and Jemal, A. (2018). Global cancer statistics 2018: GLOBOCAN estimates of incidence and mortality worldwide for 36 cancers in 185 countries. CA A Cancer J. Clin. *68*, 394–424. https://doi.org/10.3322/caac.21492.

2. Yersal, O., and Barutca, S. (2014). Biological subtypes of breast cancer: Prognostic and therapeutic implications. World J. Clin. Oncol. *5*, 412–424. https://doi.org/10.5306/wjco.v5.i3.412.

3. Riggio, A.I., Varley, K.E., and Welm, A.L. (2021). The lingering mysteries of metastatic recurrence in breast cancer. Br. J. Cancer *124*, 13–26. https://doi.org/10.1038/s41416-020-01161-4.

4. Pellegrino, B., Hlavata, Z., Migali, C., De Silva, P., Aiello, M., Willard-Gallo, K., Musolino, A., and Solinas, C. (2021). Luminal Breast Cancer: Risk of Recurrence and Tumor-Associated Immune Suppression. Mol. Diagn. Ther. *25*, 409–424. https://doi.org/10.1007/s40291-021-00525-7.

5. Ma, F., Li, H., Wang, H., Shi, X., Fan, Y., Ding, X., Lin, C., Zhan, Q., Qian, H., and Xu, B. (2014). Enriched CD44(+)/CD24(-) population drives the aggressive phenotypes presented in triple-negative breast cancer (TNBC). Cancer Lett. *353*, 153–159. https://doi.org/10.1016/j.canlet.2014.06.022.

6. Honeth, G., Bendahl, P.O., Ringnér, M., Saal, L.H., Gruvberger-Saal, S.K., Lövgren, K., Grabau, D., Fernö, M., Borg, A., and Hegardt, C. (2008). The CD44+/CD24- phenotype is enriched in basal-like breast tumors. Breast Cancer Res. *10*, R53. https://doi.org/10.1186/bcr2108.

7. Rodriguez, D., Ramkairsingh, M., Lin, X., Kapoor, A., Major, P., and Tang, D. (2019). The Central Contributions of Breast Cancer Stem Cells in Developing Resistance to Endocrine Therapy in Estrogen Receptor (ER)-Positive Breast Cancer. Cancers *11*, 1028. https://doi.org/10.3390/cancers11071028.

8. Kurtova, A.V., Xiao, J., Mo, Q., Pazhanisamy, S., Krasnow, R., Lerner, S.P., Chen, F., Roh, T.T., Lay, E., Ho, P.L., and Chan, K.S. (2015). Blocking PGE2-induced tumour repopulation abrogates bladder cancer chemoresistance. Nature *517*, 209–213. https://doi.org/10.1038/nature14034.

9. Kreso, A., and Dick, J.E. (2014). Evolution of the cancer stem cell model. Cell Stem Cell *14*, 275–291. https://doi.org/10.1016/j.stem.2014.02.006.

10. Cordenonsi, M., Zanconato, F., Azzolin, L., Forcato, M., Rosato, A., Frasson, C., Inui, M., Montagner, M., Parenti, A.R., Poletti, A., et al. (2011). The Hippo Transducer TAZ Confers Cancer Stem Cell-Related Traits on Breast Cancer Cells. Cell *147*, 759–772. https://doi.org/10.1016/j.cell.2011.09.048.

11. Park, J.H., Shin, J.E., and Park, H.W. (2018). The Role of Hippo Pathway in Cancer Stem Cell Biology. Mol. Cell. *41*, 83–92. https://doi.org/10.14348/molcells.2018.2242.

12. Creighton, C.J., Li, X., Landis, M., Dixon, J.M., Neumeister, V.M., Sjolund, A., Rimm, D.L., Wong, H., Rodriguez, A., Herschkowitz, J.I., et al. (2009). Residual breast cancers after conventional therapy display mesenchymal as well as tumor-initiating features. Proc. Natl. Acad. Sci. USA *106*, 13820–13825. https://doi.org/10.1073/pnas.0905718106.

13. Al-Hajj, M., Wicha, M.S., Benito-Hernandez, A., Morrison, S.J., and Clarke, M.F. (2003). Prospective identification of tumorigenic breast cancer cells.

Proc. Natl. Acad. Sci. USA *100*, 3983–3988. https://doi.org/10.1073/pnas.0530291100.

14. Ponti, D., Costa, A., Zaffaroni, N., Pratesi, G., Petrangolini, G., Coradini, D., Pilotti, S., Pierotti, M.A., and Daidone, M.G. (2005). Isolation and *in vitro* propagation of tumorigenic breast cancer cells with stem/progenitor cell properties. Cancer Res. *65*, 5506–5511. https://doi.org/10.1158/0008-5472.CAN-05-0626.

15. Batlle, E., and Clevers, H. (2017). Cancer stem cells revisited. Nat. Med. *23*, 1124–1134. https://doi.org/10.1038/nm.4409.

16. Chen, W., Dong, J., Haiech, J., Kilhoffer, M.C., and Zeniou, M. (2016). Cancer Stem Cell Quiescence and Plasticity as Major Challenges in Cancer Therapy. Stem Cell. Int. *2016*, 1740936. https://doi.org/10.1155/2016/1740936.

17. Plaks, V., Kong, N., and Werb, Z. (2015). The cancer stem cell niche: how essential is the niche in regulating stemness of tumor cells? Cell Stem Cell *16*, 225–238. https://doi.org/10.1016/j.stem.2015.02.015.

18. Schwabe, G.C., Trepczik, B., Süring, K., Brieske, N., Tucker, A.S., Sharpe, P.T., Minami, Y., and Mundlos, S. (2004). Ror2 knockout mouse as a model for the developmental pathology of autosomal recessive Robinow syndrome. Dev. Dynam. *229*, 400–410. https://doi.org/10.1002/dvdy.10466.

19. O'Connell, M.P., Fiori, J.L., Xu, M., Carter, A.D., Frank, B.P., Camilli, T.C., French, A.D., Dissanayake, S.K., Indig, F.E., Bernier, M., et al. (2010). The orphan tyrosine kinase receptor, ROR2, mediates Wnt5A signaling in metastatic melanoma. Oncogene *29*, 34–44. https://doi.org/10.1038/onc.2009.305.

20. Liu, Y., Rubin, B., Bodine, P.V.N., and Billiard, J. (2008). Wnt5a induces homodimerization and activation of Ror2 receptor tyrosine kinase. J. Cell. Biochem. *105*, 497–502. https://doi.org/10.1002/jcb.21848.

21. Menck, K., Heinrichs, S., Wlochowitz, D., Sitte, M., Noeding, H., Janshoff, A., Treiber, H., Ruhwedel, T., Schatlo, B., von der Brelie, C., et al. (2021). WNT11/ROR2 signaling is associated with tumor invasion and poor survival in breast cancer. J. Exp. Clin. Cancer Res. *40*, 395. https://doi.org/10.1186/s13046-021-02187-z.

22. Masiakowski, P., and Carroll, R.D. (1992). A novel family of cell surface receptors with tyrosine kinase-like domain. J. Biol. Chem. *267*, 26181–26190.

23. Roarty, K., Shore, A.N., Creighton, C.J., and Rosen, J.M. (2015). Ror2 regulates branching, differentiation, and actin-cytoskeletal dynamics within the mammary epithelium. J. Cell Biol. *208*, 351–366. https://doi.org/10.1083/jcb.201408058.

24. Kessenbrock, K., Smith, P., Steenbeek, S.C., Pervolarakis, N., Kumar, R., Minami, Y., Goga, A., Hinck, L., and Werb, Z. (2017). Diverse regulation of mammary epithelial growth and branching morphogenesis through non-canonical Wnt signaling. Proc. Natl. Acad. Sci. USA *114*, 3121–3126. https://doi.org/10.1073/pnas.1701464114.

25. Menck, K., Heinrichs, S., Baden, C., and Bleckmann, A. (2021). The WNT/ROR Pathway in Cancer: From Signaling to Therapeutic Intervention. Cells *10*, 142. https://doi.org/10.3390/cells10010142.

26. Huang, J., Fan, X., Wang, X., Lu, Y., Zhu, H., Wang, W., Zhang, S., and Wang, Z. (2015). High ROR2 expression in tumor cells and stroma is correlated with poor prognosis in pancreatic ductal adenocarcinoma. Sci. Rep. *5*, 12991. https://doi.org/10.1038/srep12991.

27. Henry, C., Quadir, A., Hawkins, N.J., Jary, E., Llamosas, E., Kumar, D., Daniels, B., Ward, R.L., and Ford, C.E. (2015). Expression of the novel Wnt receptor ROR2 is increased in breast cancer and may regulate both beta-catenin dependent and independent Wnt signalling. J. Cancer Res. Clin. Oncol. *141*, 243–254. https://doi.org/10.1007/s00432-014-1824-y.

28. Morioka, K., Tanikawa, C., Ochi, K., Daigo, Y., Katagiri, T., Kawano, H., Kawaguchi, H., Myoui, A., Yoshikawa, H., Naka, N., et al. (2009). Orphan receptor tyrosine kinase ROR2 as a potential therapeutic target for osteosarcoma. Cancer Sci. *100*, 1227–1233. https://doi.org/10.1111/j.1349-7006.2009.01165.x.

29. Xu, J., Shi, J., Tang, W., Jiang, P., Guo, M., Zhang, B., and Ma, G. (2020). ROR2 promotes the epithelial-mesenchymal transition by regulating MAPK/p38 signaling pathway in breast cancer. J. Cell. Biochem. *121*, 4142–4153. https://doi.org/10.1002/jcb.29666.

30. Bayerlova, M., Menck, K., Klemm, F., Wolff, A., Pukrop, T., Binder, C., Beissbarth, T., and Bleckmann, A. (2017). Ror2 Signaling and Its Relevance in Breast Cancer Progression. Front. Oncol. *7*, 135. https://doi.org/10.3389/fonc.2017.00135.

31. Mani, S.A., Guo, W., Liao, M.-J., Eaton, E.N., Ayyanan, A., Zhou, A.Y., Brooks, M., Reinhard, F., Zhang, C.C., Shipitsin, M., et al. (2008). The Epithelial-Mesenchymal Transition Generates Cells with Properties of Stem Cells. Cell *133*, 704–715. https://doi.org/10.1016/j.cell.2008.03.027.

32. Guen, V.J., Chavarria, T.E., Kröger, C., Ye, X., Weinberg, R.A., and Lees, J.A. (2017). EMT programs promote basal mammary stem cell and tumor-initiating cell stemness by inducing primary ciliogenesis and Hedgehog signaling. Proc. Natl. Acad. Sci. USA *114*, E10532–E10539. https://doi.org/10.1073/pnas.1711534114.

33. Thankamony, A.P., Saxena, K., Murali, R., Jolly, M.K., and Nair, R. (2020). Cancer Stem Cell Plasticity - A Deadly Deal. Front. Mol. Biosci. *7*, 79. https://doi.org/10.3389/fmolb.2020.00079.

34. Liberzon, A., Birger, C., Thorvaldsdóttir, H., Ghandi, M., Mesirov, J.P., and Tamayo, P. (2015). The Molecular Signatures Database (MSigDB) hallmark gene set collection. Cell Syst. *1*, 417–425. https://doi.org/10.1016/j.cels.2015.12.004.

35. Zhang, S., Zhang, H., Ghia, E.M., Huang, J., Wu, L., Zhang, J., Lam, S., Lei, Y., He, J., Cui, B., et al. (2019). Inhibition of chemotherapy resistant breast cancer stem cells by a ROR1 specific antibody. Proc. Natl. Acad. Sci. USA *116*, 1370–1377. https://doi.org/10.1073/pnas.1816262116.

36. John, M., and Ford, C.E. (2022). Pan-Tissue and -Cancer Analysis of ROR1 and ROR2 Transcript Variants Identify Novel Functional Significance for an Alternative Splice Variant of ROR1. Biomedicines *10*, 2559. https://doi.org/10.3390/biomedicines10102559.

37. Yu, J., Chen, L., Cui, B., Widhopf, G.F., 2nd, Shen, Z., Wu, R., Zhang, L., Zhang, S., Briggs, S.P., and Kipps, T.J. (2016). Wnt5a induces ROR1/ROR2 heterooligomerization to enhance leukemia chemotaxis and proliferation. J. Clin. Invest. *126*, 585–598. https://doi.org/10.1172/JCI83535.

38. Hasan, M.K., Widhopf, G.F., 2nd, Zhang, S., Lam, S.M., Shen, Z., Briggs, S.P., Parker, B.A., and Kipps, T.J. (2019). Wnt5a induces ROR1 to recruit cortactin to promote breast-cancer migration and metastasis. NPJ Breast Cancer *5*, 35. https://doi.org/10.1038/s41523-019-0131-9.

39. Leddon, S.A., Fettis, M.M., Abramo, K., Kelly, R., Oleksyn, D., and Miller, J. (2020). The CD28 Transmembrane Domain Contains an Essential Dimerization Motif. Front. Immunol. *11*, 1519. https://doi.org/10.3389/fimmu.2020.01519.

40. Fatma, H., and Siddique, H.R. (2024). Cancer cell plasticity, stem cell factors, and therapy resistance: how are they linked? Cancer Metastasis Rev. *43*, 423–440. https://doi.org/10.1007/s10555-023-10144-9.

41. Hung, T.H., Hsu, S.C., Cheng, C.Y., Choo, K.B., Tseng, C.P., Chen, T.C., Lan, Y.W., Huang, T.T., Lai, H.C., Chen, C.M., and Chong, K.Y. (2014). Wnt5A regulates ABCB1 expression in multidrug-resistant cancer cells through activation of the non-canonical PKA/beta-catenin pathway. Oncotarget *5*, 12273–12290. https://doi.org/10.18632/oncotarget.2631.

42. Paganoni, S., Bernstein, J., and Ferreira, A. (2010). Ror1-Ror2 complexes modulate synapse formation in hippocampal neurons. Neuroscience *165*, 1261–1274. https://doi.org/10.1016/j.neuroscience.2009.11.056.

43. Balakrishnan, A., Goodpaster, T., Randolph-Habecker, J., Hoffstrom, B.G., Jalikis, F.G., Koch, L.K., Berger, C., Kosasih, P.L., Rajan, A., Sommermeyer, D., et al. (2017). Analysis of ROR1 Protein Expression in Human Cancer and Normal Tissues. Clin. Cancer Res. *23*, 3061–3071. https://doi.org/10.1158/1078-0432.CCR-16-2083.

44. Cui, B., Zhang, S., Chen, L., Yu, J., Widhopf, G.F., 2nd, Fecteau, J.F., Rassenti, L.Z., and Kipps, T.J. (2013). Targeting ROR1 inhibits epithelial-mesenchymal transition and metastasis. Cancer Res. *73*, 3649–3660. https://doi.org/10.1158/0008-5472.CAN-12-3832.

45. Parker, B.A., Shatsky, R.A., Schwab, R.B., Wallace, A.M., I-SPY 2 Consortium, Wolf, D.M., Hirst, G.L., Brown-Swigart, L., Esserman, L.J., van 't Veer, L.J., et al. (2023). Association of baseline ROR1 and ROR2 gene expression with clinical outcomes in the I-SPY2 neoadjuvant breast cancer trial. Breast Cancer Res. Treat. *199*, 281–291. https://doi.org/10.1007/s10549-023-06914-2.

46. Jin, M.S., Kim, S.E., Heo, J.Y., Lee, M.E., Kim, H.M., Paik, S.G., Lee, H., and Lee, J.O. (2007). Crystal structure of the TLR1-TLR2 heterodimer induced by binding of a tri-acylated lipopeptide. Cell *130*, 1071–1082. https://doi.org/10.1016/j.cell.2007.09.008.

47. Lemmon, M.A., and Schlessinger, J. (2010). Cell signaling by receptor tyrosine kinases. Cell *141*, 1117–1134. https://doi.org/10.1016/j.cell.2010.06.011.

48. Bocharov, E.V., Mineev, K.S., Pavlov, K.V., Akimov, S.A., Kuznetsov, A.S., Efremov, R.G., and Arseniev, A.S. (2017). Helix-helix interactions in membrane domains of bitopic proteins: Specificity and role of lipid environment. Biochim. Biophys. Acta Biomembr. *1859*, 561–576. https://doi.org/10.1016/j.bbamem.2016.10.024.

49. Dehkhoda, F., Lee, C.M.M., Medina, J., and Brooks, A.J. (2018). The Growth Hormone Receptor: Mechanism of Receptor Activation, Cell Signaling, and Physiological Aspects. Front. Endocrinol. *9*, 35. https://doi.org/10.3389/fendo.2018.00035.

50. Maruyama, I.N. (2015). Activation of transmembrane cell-surface receptors via a common mechanism? The "rotation model". Bioessays *37*, 959–967. https://doi.org/10.1002/bies.201500041.

51. Sheetz, J.B., Mathea, S., Karvonen, H., Malhotra, K., Chatterjee, D., Niininen, W., Perttilä, R., Preuss, F., Suresh, K., Stayrook, S.E., et al. (2020). Structural Insights into Pseudokinase Domains of Receptor Tyrosine Kinases. Mol. Cell *79*, 390–405.e7. https://doi.org/10.1016/j.molcel.2020.06.018.

52. Ahmed, R.A., Alawin, O.A., and Sylvester, P.W. (2016). gamma-Tocotrienol reversal of epithelial-to-mesenchymal transition in human breast cancer cells is associated with inhibition of canonical Wnt signalling. Cell Prolif. *49*, 460–470. https://doi.org/10.1111/cpr.12270.

53. Li, M., Zheng, Y., Li, X., Shen, X., Zhang, T., Weng, B., Mao, H., and Zhao, J. (2022). ATBF1 is a potential diagnostic marker of histological grade and functions via WNT5A in breast cancer. BMC Cancer *22*, 1280. https://doi.org/10.1186/s12885-022-10380-2.

54. Park, H.W., Kim, Y.C., Yu, B., Moroishi, T., Mo, J.-S., Plouffe, S.W., Meng, Z., Lin, K.C., Yu, F.-X., Alexander, C.M., et al. (2015). Alternative Wnt Signaling Activates YAP/TAZ. Cell *162*, 780–794. https://doi.org/10.1016/j.cell.2015.07.013.

55. Dehghani-Ghobadi, Z., Sheikh Hasani, S., Arefian, E., and Hossein, G. (2022). Wnt5A and TGFbeta1 Converges through YAP1 Activity and Integrin Alpha v Up-Regulation Promoting Epithelial to Mesenchymal Transition in Ovarian Cancer Cells and Mesothelial Cell Activation. Cells *11*, 237. https://doi.org/10.3390/cells11020237.

56. Martin, M. (2011). Cutadapt removes adapter sequences from high-throughput sequencing reads. EMBnet. journal *17*, 3. https://doi.org/10.14806/ej.17.1.200.

57. Dobin, A., Davis, C.A., Schlesinger, F., Drenkow, J., Zaleski, C., Jha, S., Batut, P., Chaisson, M., and Gingeras, T.R. (2013). STAR: ultrafast universal RNA-seq aligner. Bioinformatics *29*, 15–21. https://doi.org/10.1093/bioinformatics/bts635.

58. Li, B., and Dewey, C.N. (2011). RSEM: accurate transcript quantification from RNA-Seq data with or without a reference genome. BMC Bioinf. *12*, 323. https://doi.org/10.1186/1471-2105-12-323.

59. Love, M.I., Huber, W., and Anders, S. (2014). Moderated estimation of fold change and dispersion for RNA-seq data with DESeq2. Genome Biol. *15*, 550. https://doi.org/10.1186/s13059-014-0550-8.

60. Subramanian, A., Tamayo, P., Mootha, V.K., Mukherjee, S., Ebert, B.L., Gillette, M.A., Paulovich, A., Pomeroy, S.L., Golub, T.R., Lander, E.S., and Mesirov, J.P. (2005). Gene set enrichment analysis: A knowledge-based approach for interpreting genome-wide expression profiles. Proc. Natl. Acad. Sci. USA *102*, 15545–15550.

61. Hofer, T., Tangkeangsirisin, W., Kennedy, M.G., Mage, R.G., Raiker, S.J., Venkatesh, K., Lee, H., Giger, R.J., and Rader, C. (2007). Chimeric rabbit/human Fab and IgG specific for members of the Nogo-66 receptor family selected for species cross-reactivity with an improved phage display vector. J. Immunol. Methods *318*, 75–87. https://doi.org/10.1016/j.jim.2006.10.007.

STAR★METHODS

KEY RESOURCES TABLE

REAGENT or RESOURCE	SOURCE	IDENTIFIER
Antibodies		
Monoclonal Mouse Anti- ROR2 (H1)	Santa Cruz	sc-374174; RRID: AB_10989358
Polyclonal Goat Anti-ROR1	R&D Systems	AF2000; RRID: AB_2182471
E-Cadherin (24E10) Rabbit mAb	Cell Signaling Technology	3195S; RRID: AB_2291471
YAP/TAZ (D24E4) Rabbit mAb	Cell Signaling Technology	8418S; RRID: AB_10950494
Mouse Anti-Vimentin (Clone RV202)	BD Biosciences	550513; RRID: AB_393716
Monoclonal Mouse Anti- Flag	Sigma-Aldrich	F3165; RRID: AB_259529
Monoclonal Rabbit Anti- Ki67	Invitrogen	MA5-14520; RRID: AB_10979488
Rabbit anti-Caspase-3	Cell Signaling Technology	9662S; RRID: AB_331439
Rabbit anti-Cleaved Caspase-3	Cell Signaling Technology	9661S; RRID: AB_2341188
beta Actin Monoclonal Antibody (2D4H5)	Proteintech	66009-1-Ig; RRID: AB_2687938
GAPDH Monoclonal Antibody (1E6D9)	Proteintech	60004-1-Ig; RRID: AB_2107436
Fluorescein-conjugated anti-CD44	BD Biosciences	347943; RRID: AB_400360
PE-Cy™7 Mouse Anti-Human CD24	BD Biosciences	561646; RRID: AB_10892826
PE Mouse Anti-Human EpCAM	BD Biosciences	347198; RRID: AB_400262
Alexa-647-conjugated anti-ROR2	R&D systems	FAB20641R; RRID: AB_3647738
Bacterial and virus strains		
Stbl3 Chemically Competent Cell	TransGen Biotech	CD521-01
Biological samples		
Formalin-fixed paraffin-embedded (FFPE) breast tumor tissues	Sun Yat-sen University Cancer Center	N/A
Fresh frozen breast tumor tissues	Sun Yat-sen University Cancer Center	N/A
Chemicals, peptides, and recombinant proteins		
Mouse-human chimeric monoclonal Anti- ROR2 (A12)	This manuscript	N/A
Mouse-human chimeric monoclonal Anti- ROR2 (B22)	This manuscript	N/A
Mouse-human chimeric monoclonal Anti- ROR2 (B30)	This manuscript	N/A
Mouse-human chimeric monoclonal Anti- ROR2 (B16)	This manuscript	N/A
B16 Single-Chain Fragment Variable (ScFv)	This manuscript	N/A
Critical commercial assays		
Q5® Site-Directed Mutagenesis Kit	New England Biolabs	E0554
pEASY®-Uni Seamless Cloning and Assembly Kit	TransGen	CU101
G-LISA RhoA Activation Assay Biochem Kit™	Cytoskeleton	BK124
Deposited data		
RNA-seq	This manuscript	NCBI GEO: GSE191159
The Cancer Genome Atlas (TCGA) breast invasive carcinoma (BRCA) gene expression by RNAseq	UCSC Xena	https://xenabrowser.net/datapages/?dataset=TCGA.BRCA.sampleMap%2FHiSeqV2&host=https%3A%2F%2Ftcga.xenahubs.net&removeHub=https%3A%2F%2Fxena.treehouse.gi.ucsc.edu%3A443

(Continued on next page)

Continued

REAGENT or RESOURCE	SOURCE	IDENTIFIER
GSE21974	PubMed Gene Expression Omnibus dataset	https://www.ncbi.nlm.nih.gov/geo/query/acc.cgi?acc=GSE21974
GSE87455	PubMed Gene Expression Omnibus dataset	https://www.ncbi.nlm.nih.gov/geo/query/acc.cgi?acc=GSE87455
Experimental models: Cell lines		
HEK293T	ATCC	CRL-3216
T47D	ATCC	HTB-133
MCF7	ATCC	HTB-22
MDA-MB-231	ATCC	HTB-26
HEK293F	Invitrogen	R79007
Experimental models: Organisms/strains		
Mouse: NOD-Prkdc[em26Cd52] Il2rg[em26Cd22] /NjuCrl (NCG) mice	Gempharmatech Co., Ltd	N/A
Oligonucleotides		
Primers for ROR2 mutation	This manuscript	See Table S3
Sequence of sgRNA targeting ROR2: TGCTGTGCATCCCGGCCGTC	This manuscript	N/A
Recombinant DNA		
Human ROR2 ORF plasmids	Origene	RC215640
Lentivirus vector pCDH-EF1-MCS-IRES-Puro	System Biosciences	CD532A-2
Software and algorithms		
GraphPad Prism 8.0	GraphPad Software	www.graphpad.com
ImageJ	National Institutes of Health	ImageJ.nih.gov/ij
ELDA software	https://bioinf.wehi.edu.au/software/elda/	N/A
GSEA software	https://www.gsea-msigdb.org/gsea/index.jsp	N/A
STAR aligner (v2.5.2b)	http://code.google.com/p/rna-star/	N/A
RSEM (v1.3.0)	http://deweylab.biostat.wisc.edu/rsem	N/A
DEseq2	http://www.bioconductor.org/packages/release/bioc/html/DESeq2.html	N/A
ZEN imaging software, blue edition, version 3.1	Zeiss	N/A
FlowJo_v10.6.2	https://www.flowjo.com/solutions/flowjo/downloads/previous-versions/	N/A

EXPERIMENTAL MODEL AND STUDY PARTICIPANT DETAILS

Human samples

Fresh breast tumor tissues were obtained from biopsy material of female patients (n = 67) newly diagnosed with breast invasive ductal carcinoma at Sun Yat-sen University Cancer Center, China. All of these patients were Asian, aged from 29-76 years old. Clinicpathologic features data were collected from the electronic medical records and pathology reports. Refer to Tables S1 and S2 for additional details on age and clinical information. Each of patients provided written informed consent on a protocol approved by the Institutional Review Board of Sun Yat-sen University Cancer Center, China, in accordance with the Declaration of Helsinki.

The molecular subtypes were determined by pretreatment core biopsies. Estrogen receptor (ER) and progesterone receptor (PR) status were considered positive if at least 25% of tumor cells showed ER and PR expression. Low ER-positive tumors (1% ≤ ER < 25%) were considered negative because of their clinical behavior like ER-negative tumors. HER2 overexpression (HER2⁺) was considered positive if tumor staining showed a 3+ pattern. If tumor staining was equivocal (2+ pattern), FISH was further used to confirm HER2 amplification. Luminal A subtype was defined as being ER/PRvpositive, HER2 negative, and Ki67 low (<20% cells positive) and luminal B subtype as being ER/PR positive and Ki67 high (≥20% cells positive). Triple negative subype was defined as being negative for ER, PR and HER2, as assessed via immunohistochemistry staining.

Animals

Six-to-eight-week-old female NOD-Prkdc[em26Cd52] Il2rg[em26Cd22] /NjuCrl (NCG) mice were purchased from Gempharmatech Co., Ltd and were used to generate BCA PDX. The mice were housed in laminar-flow cabinets under specific pathogen-free conditions and

their care was in accordance with the guidelines of Animal Care and use of Committee of Shenzhen University Medical School. This committee also approved all animal experiments. The experimental procedures adhered to the guidelines outlined in the National Institutes of Health Guide for the Care and Use of Laboratory Animals. The PDX models were established using mechanically minced fresh BCA specimens. Early passage (P1-P5) of primary tumor tissues from these PDX models were dissociated enzymatically/mechanically using GentleMACS Dissociator (Miltenyi Biotec), in accordance to the manufacturer's protocol. Dead cells and erythrocytes were removed via density gradient centrifugation using Percoll Plus (GE Healthcare Life Sciences, CC-17-5442-01) following the manufacture's protocol.

Cell culture
The breast cancer cell lines MCF7, T47D, MDA-MB-231 (all of female origin), and the human embryonic kidney (HEK) 293T cells were originally obtained from the American Type Culture Collection (ATCC, Manassas, VA) in 2017. These cells were maintained in DMEM (HyClone) plus 10% fetal bovine serum (FBS) (HyClone) and penicillin/streptomycin at 37°C in a humidified incubator of 5% CO_2. Human embryonic kidney HEK293F were obtained from Invitrogen and were cultured in *FreeStyle* protein-free medium (Invitrogen) in a 37°C orbital shaker containing a humidified atmosphere of 8% CO_2. The identity of each cell-line was characterized by DNA-fingerprinting and isozyme detection. The cells were passaged no more than 18 times before a low-passage batch was thawed. We added puromycin (1 μg/ml) to T47D ROR2-KO cells transduced with lentivirus empty vector or vector encoding WT ROR2 or mutated ROR2 for stable transfectants selection. Mycoplasma testing of cell cultures was carried out routinely using a MycoAlert Mycoplasma Detection Kit (Lonza).

METHOD DETAILS

Animal study
Various numbers of FACS-purified cells or cultured cell-lines were suspended in Mammary-Epithelial Growth Medium (MEGM), mixed with Matrigel (Corning, 354248) at a 1:1 ratio, and then injected into the second mammary fat pads of 6- to 8-week-old female NCG mice. Tumor formation was monitored weekly. To study the therapeutic effect of anti-ROR2 mAb on BCA, $1x10^6$ single cells isolated from PDXIII or PDXIV mixed with Matrigel (Corning, 354248) at a 1:1 ratio were injected into the second mammary pads of 4- to 6-week-old female NCG mice. 10 mg/kg control human IgG or anti-ROR2 mAb B16 were administered via intravenous injection twice a week. Tumor growth was monitored using a vernier caliper 2-3 times per week and the tumor volume was determined using the formula volume (v) = (length) × (width)^2 × 0.5. We isolated tumor cells of PDXIII or PDXIV from mice to examine the BCA cells for indicated protein expression or global gene expression at 7 to 9 weeks after treatment with anti-ROR2 mAb B16. We also re-injected these tumor cells into the second mammary fat pad of NCG female mice and monitored for 6- or 8-weeks after implantation of tumor cells for tumor engraftment using an extreme limiting dilution assay.

RNA-sequencing and data analysis
Total RNA was prepared from tumor cells isolated from PDXs using the Trizol RNA-extraction protocol with subsequent purification of RNA using RNeasy columns (Qiagen kit). Total RNA was assessed for quality using an Agilent Tapestation. Samples had RNA Integrity Numbers (RIN) ranging from 9.2 to 9.9. RNA libraries were generated from 1 μg of RNA using Illumina's TruSeq Stranded mRNA Sample Prep Kit, following the manufacturer's instructions, modifying the shear time to 5 minutes. RNA libraries were multiplexed and sequenced with 50 base pair (bp) pair end reads (SR50) to a depth of approximately 40 million reads per sample on an Illumina HiSeq6000.

We applied standard RNA-seq analytical pipeline to the sixteen samples. Briefly, adapters were removed, and reads were trimmed of bases with low quality scores in late sequencing cycles using Cutadapt, which removes adapter sequences from high-throughput sequencing reads.[56] We then mapped the reads to human genome build 38, using the STAR aligner (v2.5.2b).[57] RSEM (v1.3.0)[58] was used to obtain the raw gene counts from the read alignments and Ensemble gene models (v83). We used package DEseq2[59] to normalize the read count data and assess for differential expression. The data were deposited in a GEO database (GSE191159).

Gene set enrichment analyses
We used the GSEA software[60] for gene-set-enrichment analyses (GSEA) on PubMed Gene Expression Omnibus dataset GSE21974 and Breast Invasive Carcinoma in The Cancer Genome Atlas (TCGA) dataset that were retrieved through UCSC Xena (https://xenabrowser.net/datapages/). Of these cases, tumors with a *ROR2* expression value above the median value were designated as *ROR2*^{High}, whereas tumors with *ROR2* expression value below the median value were designated as *ROR2*^{Low}. We also performed GSEA on RNA-Seq data (GSE191159) generated from PDXIII and PDXIV isolated from mice treated with B16 or control human IgG (IgG). Each gene set was considered significant when the false discovery rate (FDR) was less than 25%. For each gene set tested, we determined the gene-set size (SIZE), the enrichment score (ES), the normalized ES (NES), the nominal p value (NOM p-val), and the FDR q value (FDR q-val). The FDR q value was adjusted for gene set size and multiple hypothesis testing.

Plasmids

Human ROR2 (WT) was amplified from ROR2 (NM_004560) human tagged ORF clone (Origene,CAT#: RC215640) and subclone into lentivirus vector CD532A (System Biosciences) by pEASY®-Uni Seamless Cloning and Assembly Kit (TransGen, CU101) according to the manufacturer's instructions. Mutated forms of ROR2 were generated with designed primers (Table S3) by Q5® Site-Directed Mutagenesis Kit (NEB, E0554) according to the manufacturer's instructions. Lentivirus vector encoding GFP and luciferase were purchased from System Biosciences (BLIV101PA). All sequences were verified by DNA sequencing.

CRISPR/Cas9 genome editing

SpCas9 and chimeric guide RNA expression plasmid lenti-CRISPR v2 vector (Addgene) were used to generate stable ROR2 knockout cell-lines. CRISPR targeting sequence (TGCTGTGCATCCCGGCCGTC) of ROR2 was designed with CRISPR Design tool (http://crispr.mit.edu/). T47D or HEK293T cells transfected with ROR2 CRISPR plasmids were stained for ROR2 using Alexa Fluor 647-conjugated anti-ROR2 (FAB20641R, R&D systems) and the ROR2-negative cells isolated and placed into culture. This process was repeated 3 successive times to isolate a population of ROR2 knock-out cells.

Immunoblot analysis

Cells were lysed in RIPA (Applygen) containing a broad-spectrum Halt Protease and Phosphatase Inhibitor Cocktail (Pierce) for 30 minutes on ice. The protein concentration was determined using a bicinchoninic acid protein assay (Thermo Fisher Scientific). Equal amounts of proteins from each of sample in RIPA were resolved by SDS-PAGE, respectively, and transferred to PVDF membranes. Then, the membranes were blocked in 5% non-fat milk, probed with primary antibodies specific for ROR2 (sc-374174, Santa Cruz), E-cadherin (3195S, Cell signaling), Vimentin (#550513, BD Biosciences), YAP/TAZ (8418S, Cell signaling), β-Actin (#66009-1-Ig, Proteintech), ROR1 (AF2000, R&D system), Caspase-3 (9662S, Cell singnaling), Cleaved caspase-3 (9661S, cell signaling) GAPDH (#6004-1-Ig, Proteintech), and then incubated with HRP-conjugated secondary antibodies (Cell Signaling). Finally, the membranes were detected with ECL reagent (Millipore) and protein bands were visualized using a Tanon-5200 Automatic Chemiluminescence Imaging Analysis System (Tanon, China).

Immunohistochemical staining

Optimal cutting temperature compound embedded fresh frozen PDX tissue sections were fixed in methonal for 20 minutes , and then were heated in 0.01 M sodium citrate buffer (pH 6.0, Solarbio, Cat#C1032) at 95°C for 15 minutes. Endogenous peroxidase activity was blocked with 3% peroxidase (ZSGB-BIO, China). The sections were blocked with 5% goat serum and then incubated with anti-Ki67 (MA5-14520, Invitrogen, 1:1000) at 4°C overnight before incubation with secondary antibodies (ZSGB-BIO, China) for 1 hour and development with 3.3′-diaminobenzidine. Hematoxylin was used to counter-stain the nuclei.

Confocal immunofluoresence analysis

Cells were cultured on glass bottom confocal dishes and then were treated without or with 150ng/mL Wnt5a for 6 hours. After washing, cells were fixed with 4% paraformaldehyde, and then permeabilized with 0.1% Trion X-100 in PBS. After washing the cells with PBS, they were blocked with 1% BSA in PBS for 30 minutes. Cells were stained with or without rabbit anti-YAP/TAZ (#8418, Cell Signaling Technology), or mouse anti-Flag (F3165, Sigma) and subsequently incubated with Alexa Fluor 594-conjugated anti-rabbit or Alexa Fluor 647-conjugated anti-mouse secondary antibodies 1.5 hours in the dark at room temperature. 4′,6-diamidino-2-phenylindole (DAPI) was used to counter-stain the nuclei before the cells were visualized under Zeiss LSM 880 Confocal Microscope.

Flow cytometry analysis

Cells were treated with Fc-blocking (Miltenyi Biotec), and then stained with Fluorescein-conjugated anti-CD44 (#347943, BD Biosciences), phycoerythrin (PE)-Cy™7-conjugated anti-CD24 (#561646, BD Biosciences), PE-conjugated anti-EpCAM (#347198, BD Biosciences), Alexa-647-conjugated anti-ROR2 (FAB20641R, R&D systems) or anti-ROR2 mAbs generated in house. Data were acquired using a FACS-Calibur or FACS-Aria (Becton Dickinson) and were analyzed using the FlowJo software (version 10.7.1). Forward light scatter (FSC) and side-light scatter (SSC) gating was used to exclude cell debris. Furthermore, we excluded cells that stained with propidium iodide (PI, Sigma) and gated on cells that stained with Calcein Violet (Life Technology) for viable cell analysis.

RhoA activation assay

RhoA activation was examined by G-LISA RhoA Activation Assay Biochem Kit™ (Cytoskeleton, BK124) according to the manufacturer's instructions. Briefly, active GTP-bound Rho in cell/tissue lysate bound to Rho GTP-binding protein linked well in 96-well plate while inactive GDP-bound Rho was removed after washing. The bound active RhoA was detected using a RhoA specific antibody. The relative degree of RhoA activation was determined by comparing OD490 value of experimental group with control group.

Cell invasion assay

5×10^4 cells that were suspended in DMEM medium containing 0.2% FBS with or without anti-ROR2 mAb or control IgG mAb (50 μg/ml) were plated in growth factor reduced Matrigel-coated invasion chambers (8-μm pore size, BD Biosciences). The lower chambers were filled with DMEM containing 10% FBS. The wells were washed with phosphate buffered saline (PBS) and fixed with 4%

paraformaldehyde after 24 hours culture. The cells on the apical side of each insert were removed by scraping. And the cells that had migrated to the basal side of the membrane were stained with crystal violet and counted using Image J software.

Cell viability assay

Cells were seeded at a density of 5,000 cells per well in 96-well plates, followed by the addition of increasing concentrations of paclitaxel the next day. Forty-eight hours later, the culture medium was replaced with fresh medium containing CCK-8 assay solution. The absorbance of each well was measured at 450 nm following a 1-2 hour incubation of the cells at 37°C in the dark. The relative cell viavbiltiy was determined by comparing OD450nm value of each well.

Spheroid formation assay

The 300-10,000 single viable cells were plated on Ultra Low Attachment 6-well or 96-well plates (Corning Incorporated Life Sciences) and cultured in MEBM growth medium supplemented with various growth factors (Lonza) for 2-3 weeks. Fresh medium was supplemented every 3 days. Spheroids with sizes greater than 100 μm were counted using an inverted microscope (Nikon).

Generation of chimeric mouse/human mAbs

An expression vector encoding hROR2 extracellular portion fused with six histidine residues were transiently transfected into HEK293F (Invitrogen) using PEI, and transfected cells were cultured in *FreeStyle* protein-free medium (Invitrogen). The extracellular portion of hROR2 was purified from supernatants using Nickel affinity chromatograph column. Two mice were immunized and boosted four times with 100 mg hROR2 extracellular portion, using Freund's complete and incomplete adjuvant (Sigma-Aldrich; St. Louis, MO). Spleens of both mice were collected and processed for a phage library (Sanyou Biopharmceuticals Co). Antibodies specific for ROR2 were selected by panning against hROR2 extracellular portion. The mAbs that have high binding affinity to hROR2 extracellular portion including A12, B22, B30 and B16, were selected for full antibodies production in HEK293F cells using human immunoglobulin G1 (IgG1) fragment crystallizable (Fc) region.and then were purified by Protein A affinity chromatography as described.[61] B16 scFv is generated by joining together the variable heavy and light chain of B16 via a peptide linker and adding 6x His tag (6 consecutive histidine residues) at C terminal. It was produced in HEK293F cells and then was purified by High Affinity Ni-TED Resin FF.

QUANTIFICATION AND STATISTICAL ANALYSIS

The number of individual animals used per group is shown by individual data points or in Figure legends. The intensity of protein bands in immunoblot analysis, YAP/TAZ located within the nuclei of the cells in immunofluoresence analysis and percentage of Ki67$^+$ cells were quantified using ImageJ. The statistical details for experiments can be found in the respective figure legends. Unless indicated otherwise, data were presented as the mean $\pm$ standard deviation (SD) of samples in triplicates in three-independent experiments. A two-tailed Student's t test was used to determine statistically significant differences between two groups. Differences between multiple groups were determined by Dunnett's multiple comparison test. All analyses were performed with GraphPad Prism version 8.0 (GraphPad Software Inc.). A P value of < 0.05 was considered significant.